THE PENNSYLVANIA STATE UNIVERSITY
SCHREYER HONORS COLLEGE

DEPARTMENT OF MECHANICAL AND NUCLEAR ENGINEERING

ESTIMATING DYNAMIC PROPERTIES FOR BIOLOGICAL MATERIALS DESIGN, DEVELOPMENT, AND CALIBRATION OF A DESKTOP MINIATURIZED PULSE-SHAPING KOLSKY BAR

KUSH BIMAL SODHA
SPRING 2016

A thesis
submitted in partial fulfillment
of the requirements
for a baccalaureate degree
in Mechanical Engineering
with honors in Mechanical Engineering

The thesis of KUSH BIMAL SODHA was reviewed and approved* by the following:

Reuben H. Kraft
Shuman Assistant Professor of Mechanical Engineering
Thesis Supervisor

Zoubeida Ounaies
Professor of Mechanical Engineering
Honors Advisor

*Signatures are on file in the Schreyer Honors College.

Abstract

Modeling and simulations are used to better understand the brains response to external loading. Modeling requires supplying the mathematical description of the tissue behavior, or constitutive model, as well as its material properties. We seek to examine the performance of existing methods and develop new methods in order to characterize the mechanical properties of the tissue used in models of the brain. Recently, there have been concerns regarding the validity of using the Kolsky bar to acquire mechanical properties of soft, biological materials at high strain rates. This effort further explores the validity of the Kolsky bar for soft materials.

Currently, Kolsky bars are too large and geared towards testing traditional engineering materials such as metals or ceramics. Using the known mechanics of the Kolsky bar in engineering materials, we aim to miniaturize the model to eliminate some of the inertial effects and employ pulse shaping to further address the compressible nature of the specimens. Even with these alterations, additional testing including shear mechanisms to develop a shear modulus and changing specimen geometry remain possible options to fully optimize the response of soft materials.

In order to explore the validity of the Kolsky bar, we employ solid and computational modeling to evaluate different materials tested in miniaturized Kolsky bar apparatus. Our approach started by developing a miniaturized compression model in Solidworks. We then developed and refined a finite element mesh using Ansys ICEM-CFD. With a high-quality mesh, we employed LS-DYNA to conduct the dynamic simulations of the experiment. The material properties assigned start with aluminum cylindrical specimens, but are then transitioned to a softer material.

Understanding the weaknesses with the soft specimens prompted the use of pulse shaping. This analysis can prove the validity of using Kolsky bars with modifications on soft, biological materials. Combining these mechanical properties with existing models for the human body can expand the current understanding of the brains response to high-strain rate loading and aid in prevention, treatment, and rehabilitation of TBIs.

Table of Contents

List of Figures

List of Tables

Acknowledgments

This publication would not have been possible without the help and support of all the members and faculty involved with the Penn State Computational Biomechanics Group. A special thanks goes to Dr. Reuben Kraft, the head of the group, and all of his graduate students. This research also benefited from funding and support from the College of Engineering Research Initiative and its Research Experience for Undergraduates for Summer 2015. I would also like to thank my family for their understanding and support while I worked on this project at the Pennsylvania State University in State College, PA.

Chapter 1

Introduction

Understanding the mechanism and dynamics of a Kolsky bar along with the motivation to find a way to measure more accurate high-strain rate soft material properties is key to understanding this research. In this chapter, the workings of a Kolsky bar are explained to provide some high level background as we delve into modifying the Kolsky bar for soft materials. In addition, a little information is also given about the need and motivation for research like this undertaking.

1.1 Background

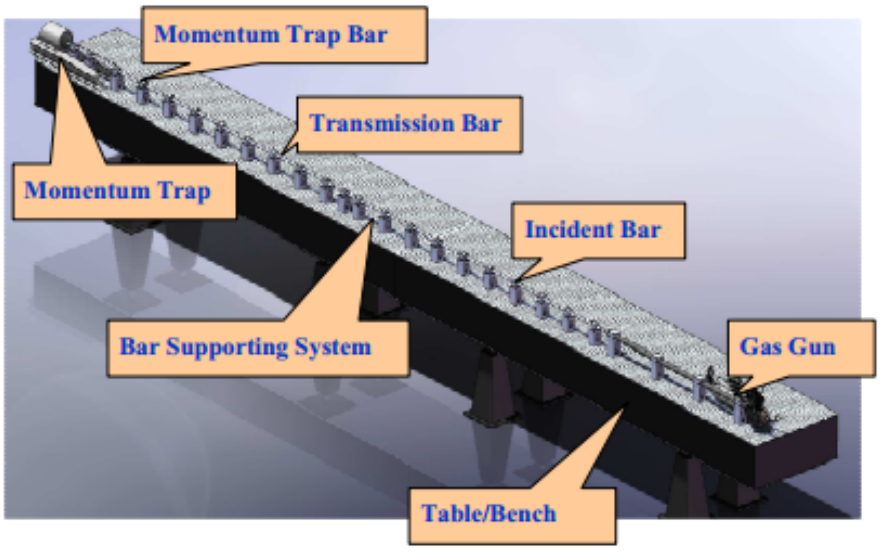

Figure 1.1. Kolsky Bar Setup [1]

The split Hopkinson pressure bar, also known as the Kolsky bar, was the first apparatus capable of generating a complete stress-strain curve for high strain rate loading. Created in 1962, the Kolsky bar (Figure 1.1) has been used to evaluate the behavior of a wide range of materials including ceramics, but has only been applied to brain tissue and other biological material in the last ten years [9]. Soft materials are characterized by the ratio of their bulk to shear modulus. In the transition to liquids to solids this ratio grows almost exponentially to infinity. In liquids, the shear stress is almost zero. Soft materials are defined by having such low shear stresses such that the ratio of bulk modulus to shear modulus is estimated in the range of $10^4 - 10^7$ [10]. Having this ratio allows estimation of the Poisson's ratio and define the range of soft materials.

This project aims to use the principles of this apparatus to more accurately estimate the mechanical properties of biological materials under high rates of strain. Using this test apparatus and calibrated test data to establish properties of softer materials at high strain rates could expand researchers current knowledge about the response of biological materials and enhance the existing finite element models used to model high strain rate impacts on brain tissue. Developing a test apparatus that can more accurately predict the material properties of the brain at high strain rates in conjunction with existing finite element models of the brain would allow for better defense from, alleviation of, and recuperation from injuries that range from concussive hits in football and automotive crashes to ballistic impacts and blast overpressure loadings [2].

Figure 1.2. Illustration of parts included in Kolsky Bar model

In addition to the overall goals of the project, it is important to understand the basic function of the device pictured in Figure 1.2. Currently up to 5 meters in length, Kolsky bars allow us to estimate the material properties of a specimen suspended between two very long bars to eliminate inertial effects. A pressure powered gas gun provides an initial velocity to a shorter striker bar - the first in a series of three bars. From this preliminary impact, the velocity is imparted onto an incident bar which receives the impact and transfers it onto the specimen. The

third and last bar is the transmission bar which moves with the specimen to allow the specimen to be elastically loaded. The last part is a stopper or momentum trap that absorbs the kinetic energy of the transmission bar. Traditionally located in large rooms, tests are performed over a short period of time determined by the material properties of the bar. Strain gages placed in close proximity to the specimen on the incident and transmission bar measure strain values in the axial direction. Using these strain measurements and the material properties of the bar, an estimate of the stresses and strains in the specimen are generated. Combining these values allows for an estimation of common material properties like Young's modulus or nonlinear elastic properties at high strain rates [1]. A few modifications to this design discussed below can adjust this procedure to soft materials.

Through design modifications, traditional Kolsky bars can be adopted to test softer materials and measure their material properties. Although all of these design modifications are not fully explored, the logical ones have been tested. With some combination of these alterations, the hope is to achieve uniaxial loading for the soft material case. By guaranteeing this uniaxial assumption, we can use the strain gages attached to the incident and transmission bars to accurately estimate specimen material properties. Without this criterion of uniaxial specimen stress satisfied, any correlation between the strain in the bars and the material properties of the specimen is invalid.

Currently, Kolsky bars that measure the material properties of metals and ceramics under high strain rates are sized to minimize wave dispersion and inertial effects to mimic uniaxial loading. Machine dimensions, a function of specimen length and diameter, normally range from a length of 0.7-1.3m for each bar. Ramesh provides a strategic shift aimed at modeling higher strain rates through a decrease of the specimen length, direct impact on the specimen (thus increasing effective velocity), and miniaturization of the entire system [11]. The first modification uses a miniaturized, desktop Kolsky bar with a length of 0.3m per bar. It will help reduce the size and thickness of the brain tissue specimen by overcoming the excessive deformation in softer materials in comparison with metals and ceramics.

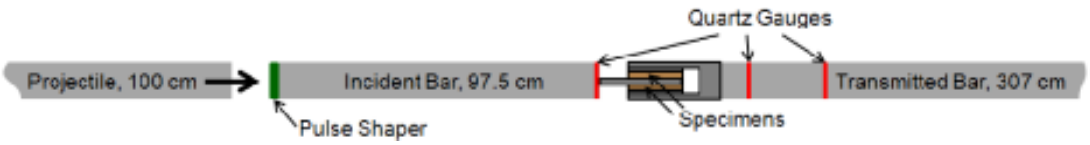

Figure 1.3. Double-lap Shear Kolsky Bar Apparatus [2]

Traditionally Kolsky bars are also used to measure a materials dynamic properties (strain rate 103-104 s^{-1}) through compression loading but as the Kolsky bar became the standard, tension and torsion models were also developed. Fields [12] goes on to explain pressure-shear plate impact that can be used to model even higher strain rates. However, the adjusted Kolsky bar would test shear rather than compression and provide a shear modulus rather than a traditional Young's modulus that can be imperative in understanding impact in a new way. Knowing that these material properties can be strain-rate dependent also applies to shear loading. Given the wide range of shear loading with peak shear strains of up to 45% and peak strain rates of 105 s^{-1}, a Kolsky bar is a perfect way to chart these strain-rate dependent material properties across this range of shear [13]. The second modification to the Kolsky bar arises from a merger of these two concepts a double lap shear loading that still uses the incident bar and transmitted bar of a Kolsky bar apparatus (Figure 1.3).

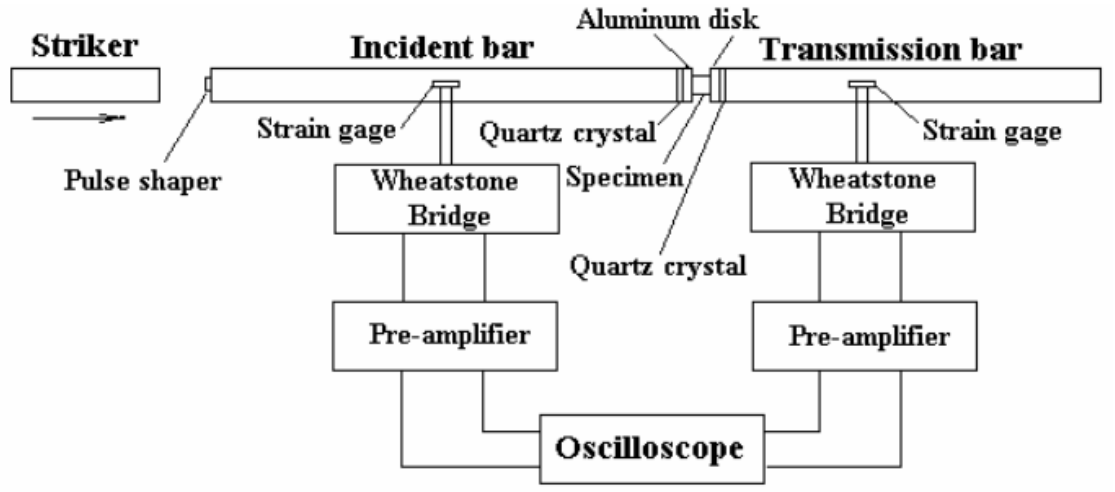

Figure 1.4. Possible Placement of Pulse Shapers in Kolsky Bar Model [3]

Another recommended change that can adapt existing Kolsky bars to softer materials is pulse shaping of the initial impact. Traditionally all of the stresses from the striker bar are continuously transferred onto the incident bar which begins a stress wave that propagates through the incident bar onto the specimen. This method allows all of the stresses at any frequency to reach the specimen. For soft material, this method allows very high stresses to reach the specimen that generates failure before the entire response can be examined [7]. Pulse shaping can help with this anomaly in two ways - it removes the oscillation in the pulses

providing a high signal-to-noise ratio for the sampling and it attenuates the initial incident pulse by spreading it over time rather than one impulse [3]. Pictured in Figure 1.4, Song's portrayal of pulse shapers in a Kolsky bar apparatus allows for better simulation results for soft materials.

In addition to these three design changes, Ramesh also suggests using precise equipment including bars with small elastic moduli and piezoelectric quartz gages to improve accuracy [11]. Through these modifications, the aim is to propagate an absolute uniaxial stress state in soft, biological materials. Getting more accurate results for specimen material properties can have widespread impact in the field of biomechanics and specifically at the Penn State Computational Biomechanics Laboratory here at Penn State. Combining these strategies can allow us to validate the feasibility of the model.

1.2 Motivation

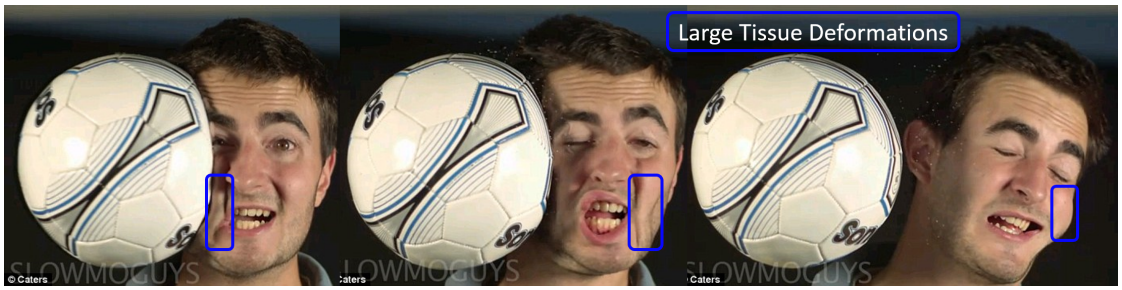

Figure 1.5. Slow Motion Image Capture of Soccer Ball Collision [4]

Traumatic brain injuries can be seen in many different walks of life, including combat operations. Figure 1.5 shows a slow motion camera capture of a soccer ball impact to show the minuscule time intervals in which high strain rate impact occurs. Although commonly pictured in sports scenarios, these high strain rate loadings onto the body are ever present in military operations and can even be seen in car collisions. Additional knowledge and improved models can be the key to impacting the current understanding and treatment of traumatic brain injuries, referred to as TBIs, caused by such impact to the brain [14]. The U.S. Department of Health and Human Services estimates that 1.7 million TBIs occur in the United States annually [15]. TBIs commonly induce high rates of loading to the tissue known to be rate-dependent [16].

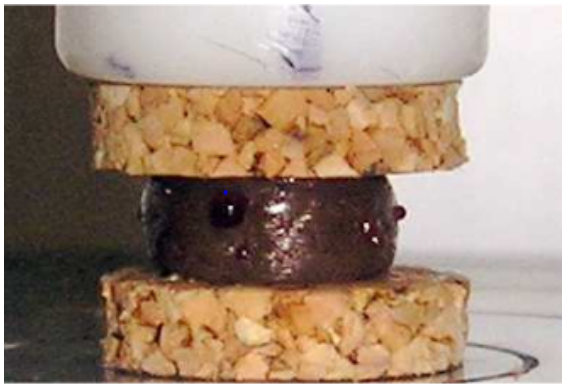

Figure 1.6. Compression Testing for Liver Tissue [5]

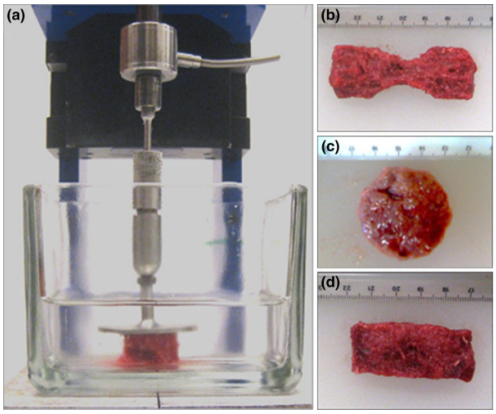

Figure 1.7. (A) Mechanical Testing Mechanism for Placenta Samples in (B) Tension, (C) Compression, (D) Shear [6]

The Penn State Computational Biomechanics Group develops several predictive models for injury and disorder in many different parts of the human body. Ranging from predictive models that deal with traumatic brain injury and spinal cord damage to lower extremity injuries, but these models are only as good as the numerical dynamic material properties that are used. Through this exploration, we aim to improve existing estimates of dynamic material properties of soft, biological materials at high strain rates.

There are many working models for low strain-rate loading for many different parts of the body. Figure 1.6 shows experimental testing on the liver tissue in compression loading undertaken at the University of Cincinnati, while Figure 1.7 shows failure in different modes of testing for placenta samples. Although there are many experimental results for soft tissue material properties within normal loading and strain rates like the ones shown above, this data for high strain rate applications is lacking [17]. High rate strain material properties are especially effective and useful in several impact simulations. A better understanding of these impact scenarios can lead to better predictive models which can assist in the treatment of injuries from blasts, car crashes, and even concussive injuries. In addition to evaluating the feasibility of this miniaturized apparatus for soft materials at high strain rates, the plan is to assemble this device in the lab to avail other projects of high strain rate dynamic material properties for soft, biological materials.

Chapter 2

Dynamic Finite Element Analysis Process

The next step after establishing some background for the Kolsky bars and the importance of an endeavor to find more accurate high strain-rate material properties is the process developed and the required software for this undertaking. The next few section outline the necessary steps taken to create computational models of the Kolsky bar. This chapter focuses on an overview of the process and the phases involved.

2.1 Computational Modeling Process

In order to evaluate the miniaturized Kolsky bar, an iterative process was established that would give us a numerical measure of the uniaxial state of stress. A uniaxial stress state is important to accurately evaluate the dynamic material properties of a Kolsky bar. In the Kolsky bar apparatus material properties are estimated from a pair of strain gages attached to the incident bar and the specimen bar as seen in Figure 1.2. The strain gages are connected to a Wheatstone bridge or an optical device that amplifies and displays the strain in the bars. Using the material properties of the bar, the strain is projected onto the specimen and accounting for the projected velocity the dynamic material properties are estimated. In order to translate the strain, the stress state needs to be uniaxial to avoid inaccuracies [1]. In order to test for the nature of the stress state computationally, a iterative procedure is outlined in the next few chapters starting

with computer-aided design, going through finite element modeling, and concluding with dynamic computational simulation. The following sections explain the methods and technology used in this endeavor as outlined in Table 2.1.

Table 2.1. Computational Modeling Process Overview

Computational Modeling Process		
Stage	Software	Purpose
Computer Aided Design	SolidWorks	Design Changes
Finite Element Meshing	ANSYS ICEM-CFD [17]	Refining Mesh Quality
Dynamic Simulation	LS-DYNA [18]	Develop Constitutive Model

2.2 Computer Aided Design: SolidWorks

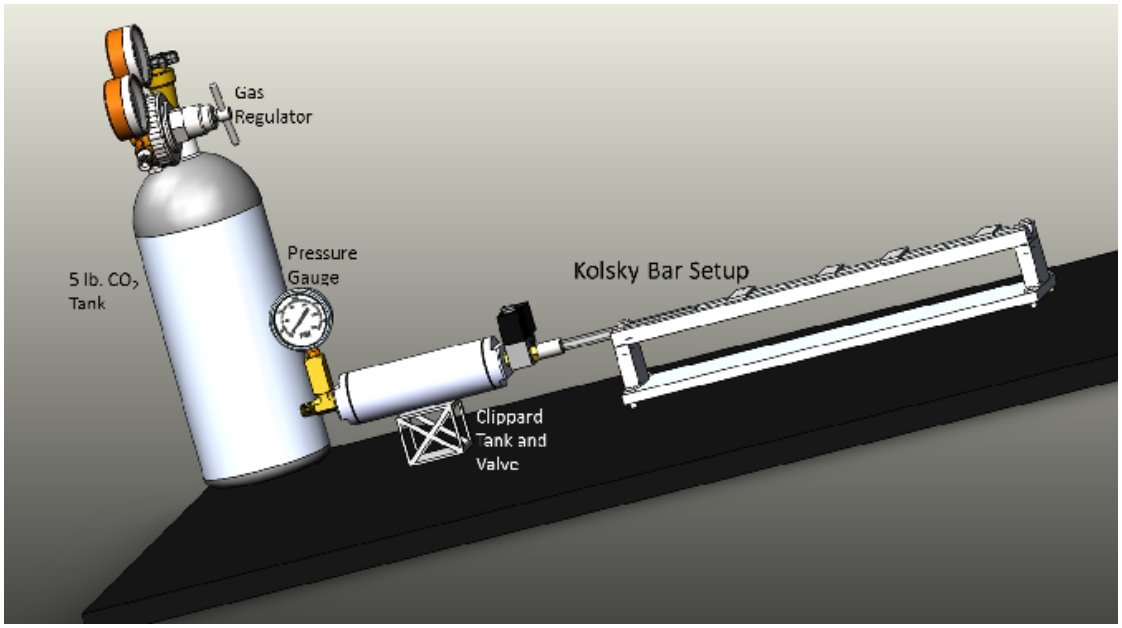

Figure 2.1. CAD Model of Miniaturized Kolsky Bar Setup

The model of the miniaturized Kolsky Bar Setup shown in Figure 2.1 began with scaling the dimensions to fit a predetermined space in the Computational Biomechanics Group lab at Penn State. Developing this model in SolidWorks was mostly done with CAD models of existing parts and systems. This is beneficial for two reasons - the cost reduction associated with existing parts and the ease of assembly from these preexisting parts. The miniaturized model contains all of the

components of the full model with severe size reduction (about 20x) to the bars in the assembly. The Kolsky bar setup has three bars and a cylindrical specimen. The bars in contact with the specimen are each 150 mm in length and the specimen is 0.2 mm thick pictured in the setup in Figure 2.2. This scale allows for minimization of dispersion and inertial effects. The hope remains that the reduction of mass and inertial effects will help maintain a uniaxial stress state.

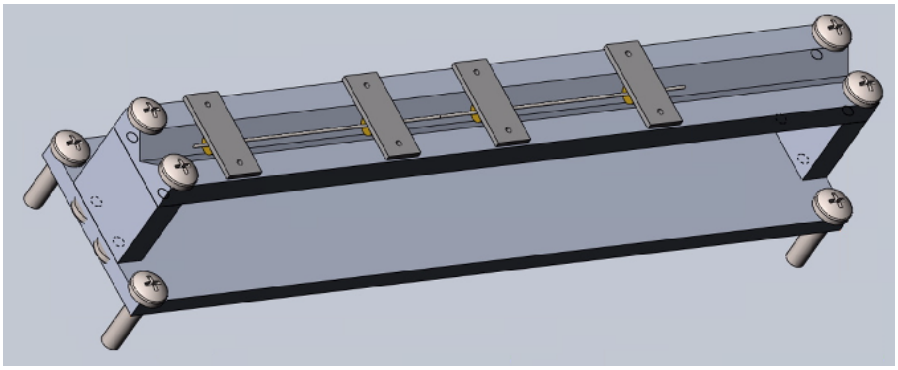

Figure 2.2. Detailed View of the Bars in the Setup

2.3 Finite Element Meshing: ANSYS ICEM-CFD

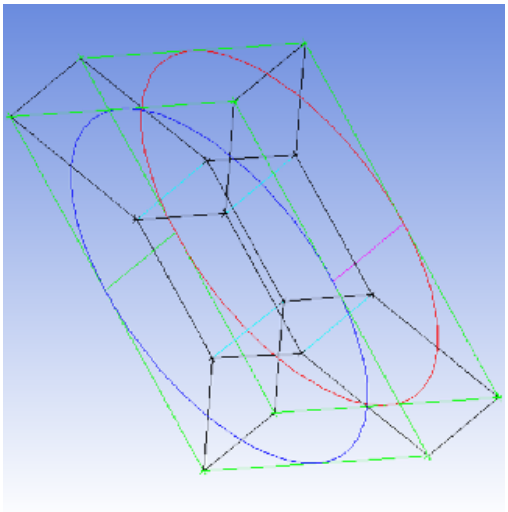

Figure 2.3. O-Grid Blocking Pattern for Unstructured Mesh

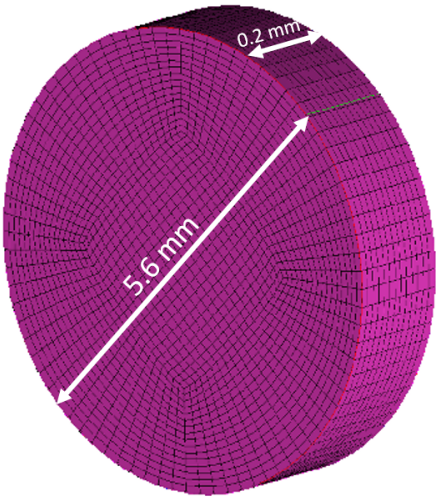

Figure 2.4. Complete Volume Mesh of Cylindrical Specimen

The second step of the process involved breaking up the four important bars of the setup into finite elements for further testing and analysis of the stress state

at different points in the specimen. The meshing started with an automatically generated hexagonal mesh, but this mesh did not allow enough resolution and consistency for the stress state along the radius of the specimen. In order to smooth the results, we changed the dimensions of the blocks, shown in Figure 2.3, as well the number of elements along certain axes to refine a few mesh quality metrics. Appendix A includes the spread of all the metrics used to evaluate the overall mesh quality. Of the six metrics, orthogonality and skew were optimized the most for cost and time constraints. Computational simulation requires high speed computing, which is time-intensive and expensive, so controlling these two facets is an important consideration of the overall mesh quality. Refining the mesh to the level shown in Figure 2.4 helped achieve accurate and consistent results for the outer blocks. After the meshing was resolved and the components were repackaged, the ANSYS mesh could be exported to LS-DYNA for numerical, computational simulation [17].

2.4 Numerical Computational Simulation: LS-DYNA

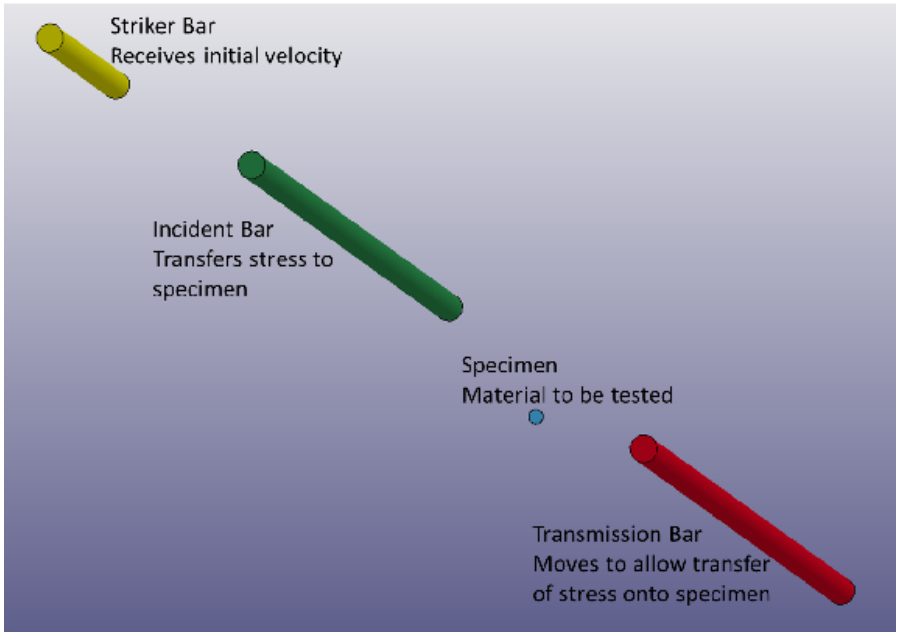

Figure 2.5. Finite Element Meshes of Major Parts for Computational Simulation

The last step in the first iteration of this process was importing the meshes into LS-DYNA by part as demonstrated in Figure 2.5 and defining the part parameters

to simulate impact. ANSYS predefines certain keywords, but there are a few major keywords that need to be defined in order to accurately run the collision simulations. Six important keywords were adjusted for high strain rate impact for soft materials - boundary, termination, mat, contact, initial, and section.

The first parameter - boundary - was set along the very center node along all the bars. The boundary condition being set was setting only one axis of freedom in the axial direction. This had to be done for all the parts to avoid any influence of gravity or random motion might have on the specimen. This is accomplished in the CAD model by annular holders that keep the bars in place only allowing motion in the axial direction.

The termination keyword was set by the rate of stress propagation through the incident bar. The speed of stress propagation is defined by:

$$c = \sqrt{\frac{E_{bar}}{\rho_{bar}}} \tag{2.1}$$

Using this speed and the known length of the bar, the transmission time of one pulse can be found. Their termination time, however, is set as twice this value, 60 μs to account for one complete reflection of the stress wave in the incident bar.

LS-DYNA is equipped with good contact algorithms and out of the available ones, automatic general contact was picked.

The last keyword, mat, was defined as an elastic model of the material of each of the bars. The bars were always defined as aluminum, a traditional engineering material, but the specimen was alternated between aluminum, a standard engineering material, and the elastic material properties of brain tissue determined experimentally.

The impact velocity of the striker bar also needed to be set in order to get the desired high strain rate. Strain rate is commonly to be a function of the impact velocity and specimen diameter.

$$\dot{\varepsilon}_{desired} = \frac{v_{striker}}{d_{specimen}} \qquad v_{striker} = \dot{\varepsilon}_{desired} d_{specimen} \tag{2.2}$$

Given the specifications of a desired strain rate of 3000 Hz and a specimen diameter of 5.6 cm, the sensible choice for impact velocity was determined to be 15 m/s. Although this might not seem like a high velocity, it is magnified by the

miniaturized specimen and the bigger staple here is maintaining a high strain rate even at this level.

The last keyword that was manipulated several times to account for soft tissues was the section type used in the meshes to compute stresses and strains. LS-DYNA automatically loads on a constant stress state solid onto the mesh imported from ANSYS-ICEMCFD. However, there are some modifications necessary to this automatic designation for engineering materials versus soft materials to allow better results and accurate failure modes. For engineering materials, the optimal setting is eight points in each volume integrated continuously. Such an analysis is accurate for the bars in each simulation as well as the aluminum specimen. For softer materials, the optimal setting was found to be an ambient Eulerian-Lagrangian integration method over the specimen. This allows mitigation of the stiff hourglass control and the appearance of negative brick volume elements [18].

In addition to these specifications, a time history of 27 elements located halfway along length of the specimen and along the radius of the specimen was logged in a binary output file for a hundred time intervals.These adjustments to the keyword file allowed for results that reflect the entire length of the specimen and its stress state. A sample keyword file used for dynamic modeling and numerical simulation is included in Appendix A with all of the values listed above as well as the selection of material properties listed below.

2.5 Defining Testable Material Properties

One of the most important keywords defined above is the mat keyword in LS-DYNA. This keyword allows us to set multiple materials in a simulation and assign these material properties to different parts. Although the material properties of engineering materials are readily available for many engineering materials the information for brain tissue was harder to find. LS-DYNA uses a combination of density, Young's modulus, and Poisson's ratio to define the material properties of an element. For aluminum, these values were determined to be a density of 2712 kg/m^3, a Young's modulus of 69 GPa, and a Poisson's ratio of 0.334.

Finding testable properties that were under similar conditions as the specimen being tested was a challenge. Due to the scarce nature of material properties at high strain rates, a lot of existing literature with different experimental techniques

was analyzed and compared to find the closest fit to the operating conditions in the miniaturized Kolsky bar. The first step in the process was finding density of a material comparable to brain tissue. There are several older journal articles which experimentally measure the density of brain tissue, but the one that fit our needs was Barber's study performed on brain tissue which yielded a density of 1043 kg/m^3 [19]. Once the density of the specimen was set, the next step was to find an acceptable range for brain tissue elastic modulus and Poisson's ratio. For this search, the high strain rate condition was imperative so an accurate range could be found to compare our analytical results to. The Poisson's ratio predicted in similar situations was identified to be in a range from 0.4 to 0.499 [20]. Throughout the experiments four of the six computational specimens tested satisfied this criteria. Additional research into loading rates to compare to strain rates and limiting the type of loading to compression loading identified a value for the Young's modulus of brain tissue - 10 MPa [21]. In stark contrast and magnitudes lower than the Young's modulus of Aluminum, this value was paired with the highest Poisson's ratio in the sample that most represented brain tissue.

2.6 The Transition from Aluminum to Brain Tissue

Table 2.2. Material Selection Process Overview

Specimen Input Material Properties			
Specimen	Density (kg/m^3)	Young's Modulus (MPa)	Poisson's Ratio
Aluminum	2712	69000	0.33
Sample 1	2250	30000	0.37
Sample 2	2000	10000	0.41
Sample 3	1500	1000	0.45
Sample 4	1200	100	0.47
Brain Tissue	1043 [19]	10 [21]	0.49 [20]

Since the material properties of aluminum and brain tissue are so vastly different it is important to go deeper than just a direct comparison between these two materials. In order to more closely examine the difference between these two contrasting materials at high strain rates, four additional specimen sample material properties were generated for intermediate values between these two materials as shown in Table 2.2. Understanding the degrees of variance in the properties and their meaning allowed for a more meaningful transition. All of the properties were

interpolated either logarithmically or asymptotically to allow for more samples closer to the likeness of brain tissue.

2.7 Plastic Yielding Setup

In order to do model a pulse shaper have to be repeated including computer-aided design, meshing and the numerical and dynamic simulation. Before running any simulations, though, the details of how copper yields is necessary to continue. Defining the yielding includes defining a yield point and yield behavior in addition to the Young's modulus charted at different temperatures in Figure 2.6. LS-DYNA requires a combination of the elastic and plastic regions of yielding for copper to get a complete description of the material used in the pulse shaper.

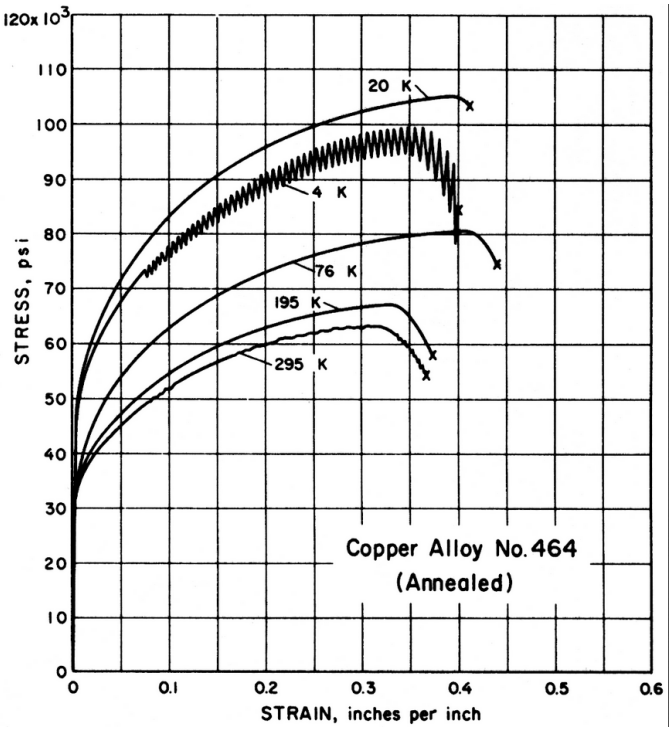

Figure 2.6. Elastic and Plastic Yielding of Annealed Copper Samples

2.8 Geometry and Location of Pulse Shaper

Despite the many possible configurations of the pulse shaper, the first one to be tested is demonstrated and used in the model is referenced and used in Scheidler,

Fitzpatrick, and Kraft [7] as well as Song and Chen [3]. Using a placement agreed by these two independent papers, the pulse shaper was determined to be placed in between the striker and the incident bar as shown in Figure 3.7. This positioning of the pulse shaper allowed for easy insertion into the current model, and created a buffer between the pulse shaper and the specimen.

Figure 2.7. Positioning of Pulse Shaper in the Model

In addition to identifying the material and the position, geometry was also an important factor to consider. Choosing a circular or annular specimen and its scale compared to the bar faces was a tough decision. Ramesh [11] recommended the use of a circular pulse shaper, and upon further analysis the pulse shaper was adjusted to be a little smaller in diameter than the bar faces, just as the specimen is.

Chapter 3

Miniaturization Analysis and Results

This chapter outlines the steps used in verifying the finite element analysis of the Kolsky bar. In order to ascertain that the computational modeling of the Kolsky bar simulated the physical system accurately, velocity, stresses, and strains at important locations were confirmed with expected outcomes. This process also helped understand the important times within the simulation where the model would deviate most from a uniaxial stress state.

3.1 Existing Results

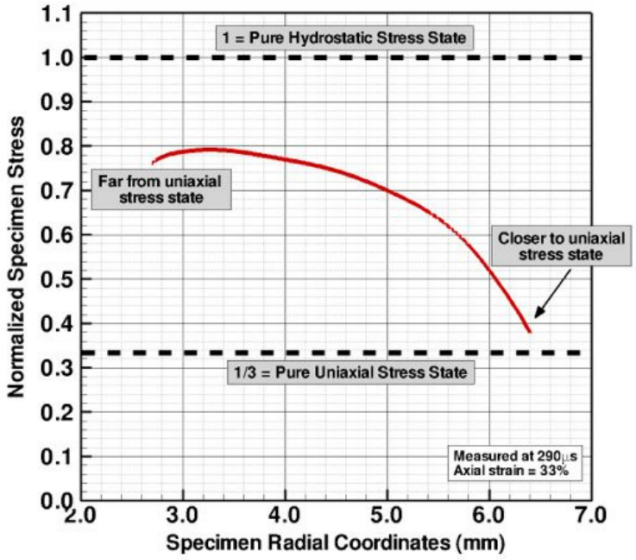

Figure 3.1. Normalized Stress over the Specimen Radius [7]

Previously, full-sized Kolsky bars have been used to sample biological materials with huge deviations from the uniaxial stress state. Figure 3.1 shows the results of a computational analysis of the uniaxial nature of the impact in the Kolsky bar. The bottom dotted line signifies a purely uniaxial stress state whereas the top dotted line signifies a purely hydrostatic stress state. The normalized stress begins far away from the uniaxial state and eventually gets close to the uniaxial line [7]. The problem identified is how the inner third of the specimen deviates strongly from the uniaxial assumption necessary to obtain specimen material properties. Using our miniaturized model and other possible changes, the aim is to lower the radial and hoop stresses in the specimen by removing inertial effect to restore the system to a uniaxial stress state.

3.2 Model Viability

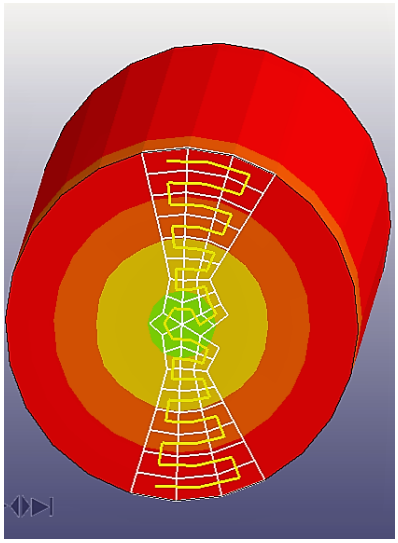

Figure 3.2. Method to Accurately Estimate Axial Stress at a Point

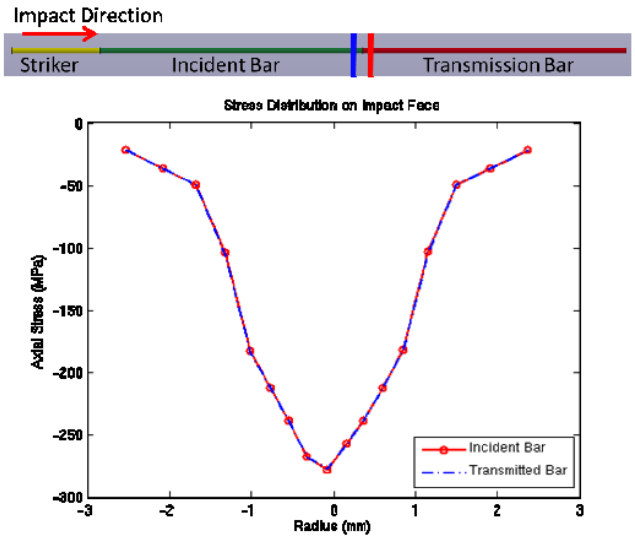

Figure 3.3. Establishing Dynamic Equilibrium

The first test performed on the model was to establish dynamic equilibrium. Figure 3.2 shows an analysis of the determination of the stresses near the bar. A snake method was used with three elements at each radius, r, away from the center. Averaging these three values gave us an accurate estimate of the stress at each radius. This simply means verifying that the forces on either side of the specimen are equal to each other. In order to establish this, stresses were analyzed

2 mm away from the specimen edge on both the incident bar and the transmission bar. Shown in Figure 3.3, the results of this test were what we expected them to be. Given the identical nature of the stresses, we could move on to another tests to identify the exact time at which the stress on the specimen reached the maximum. This equivalence of dynamic equilibrium allows us to assume that the strain rate dependency and wave propagation of the specimen can be a function of just one of the bars at the instant in time where the maximum stress occurs. This helps us simplify our understanding of the strain rate in relation to bar material properties and estimate specimen material properties from parts of the bar nearest to it. Following the establishment of dynamic equilibrium, several velocity analyses were used to get a better understanding of the model.

3.3 Velocity Analysis

In order to understand the loading on the specimen and more accurately explain the motion of the bars in the Kolsky bar assembly, there were a few studies of the velocities at different locations and times along the incident bar to understand the complete motion of this assembly. The first velocity analysis done to study the loading onto the specimen was the velocity at the incident bar end pictured in Figure 3.4. Figure 3.5 catalogs the results of velocity analysis with the initial ramp up as well as the oscillations from the loading onto the bar.

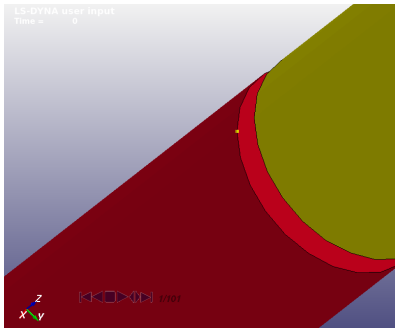

Figure 3.4. Incident Bar Velocity Location

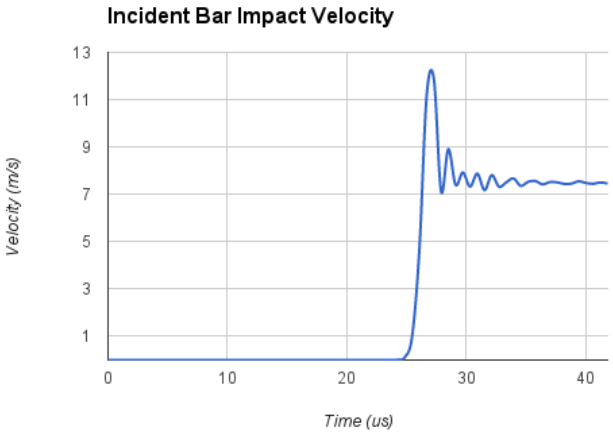

Figure 3.5. Incident Bar Impact Velocity

Once analysis of the incident bar velocity over the span of the simulation was complete, a more thorough analysis of the velocity of both bars was undertaken. In

order to get a complete picture, elements close to the center were picked as shown in Figure 3.6 and averaged to gain a estimate for the time at which the velocity difference between the bars was greatest. Figure 3.7 also shows a comparison of the two bar velocities over time. The time at which the velocities deviate most is an expression of the instant at which the loading on the bar is maximized. This maximum compression of loading offers maximum compression and in turn maximum strain. Since an elastic model is used, this maximum strain also corresponds to a maximum stress. Dynamic modeling shows that this maximum stress is where the model deviates the most from the uniaxial stress assumption. According to the plot below, this occurs roughly at 25 μs.

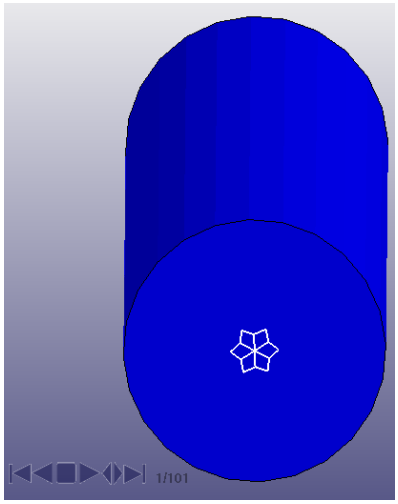

Figure 3.6. Method to Accurately Estimate Axial Velocity of Bars

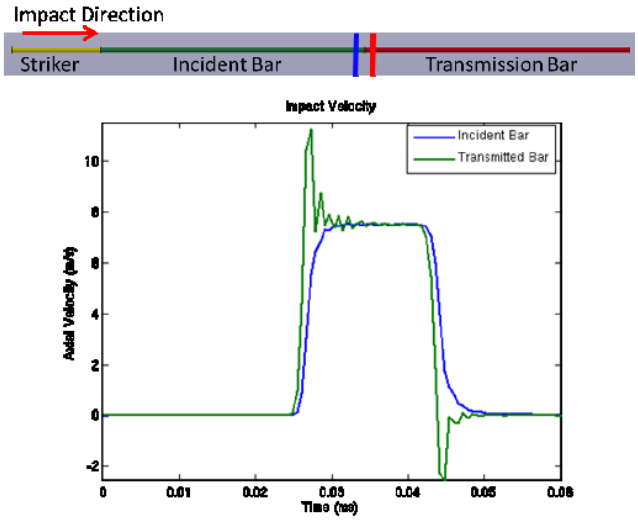

Figure 3.7. Establishing a Relationship between Bar Velocities

3.4 Wave Propogation

In addition to understanding the relationships between the incident bar and the transmission bar velocities as well as the initial loading on the incident bar, wave propagation is a key to understanding simulation time. A sample simulation for ten time intervals within the simulation time shows how the wave travels through the specimen and also how it is reflected. The specimen impact starts around the sixth snapshot of Figure 3.8 ($\sim$30 μs), and the first reflected wave begins propagating at the ninth snapshot of Figure 3.8 ($\sim$48 μs). An ideal simulation time would include

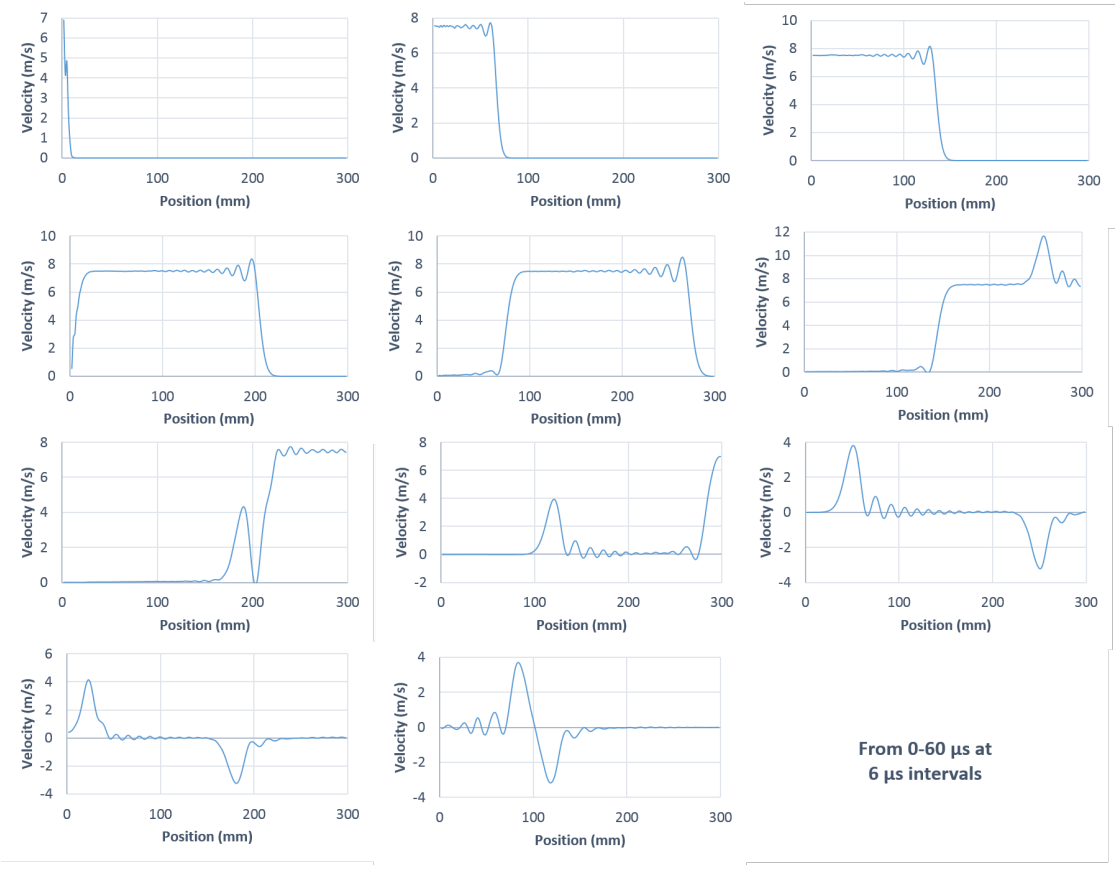

Figure 3.8. Analyzing the Velocity Distribution over the Incident Bar

one cycle of a wave which returns to the side of the incident bar away from the specimen. Understanding how this wave propagates and when a reflective cycle is complete is not only important in identifying a termination time, but also key in understanding where the maximum strain occurs and the point from which to obtain specimen data for the feasibility analysis.

3.5 Simulation Times and Completion Percentage

The starting point for each simulation was using the standard LS-DYNA constant stress state solid. Understanding the computational needs for this simulations and its correlation to completion percentages was key in understanding how more complicated models would run, and identify some of the weaknesses of using the constant stress state for advanced analysis. The first thing of note in Figure 3.9 is that when the simulation fails before completion for the two softest materials

listed in Table 3.1 the simulation time is a fraction of when it runs a complete simulation. Analysis of the failure is not a strength of the simple analysis in constant stress state solids. Another key observation is the noisy feedback of stress along the elements and voids and deformations formed in the elements. Of the completed simulations, the simulation time decreases as we progress towards traditional engineering materials as expected.

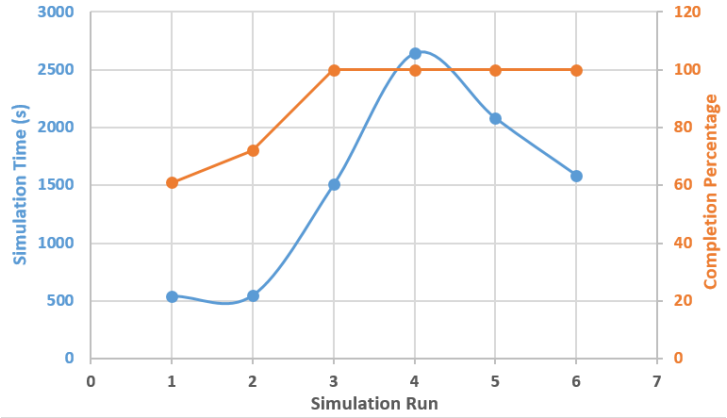

Figure 3.9. Budgeting Computational Time

Table 3.1. Simulation Materials

Simulation Run Correlation	
Run	Material
1	Brain Tissue
2	Sample 4
3	Sample 3
4	Sample 2
5	Sample 1
6	Aluminum

3.6 Identifying Deviation from Uniaxiality

Using a similar approach as analyzing the completion time, the constant stress state solid simulation runs were once again analyzed for all materials listed in Table 3.2 for an analysis of when the biggest deviation from uniaxiality happens. In combination with comparing the bar velocities, this maximum strain analysis can provide a best practice time period to test for deviation form the uniaxial stress state.

Maximum specimen strain in this scenario is classified as the maximum strain at any point in the specimen. Although the strain in the elements being measured might be slightly different, the maximum strain was considered as the benchmark for this analysis. Another consideration is the low strains when we approach aluminum specimens. Since the bars are also made of aluminum, there is not an appreciable difference between the stiffness to cause a buildup of strain. Aluminum specimens had to be analyzed with steel bars in some past experiments to overcome this obstacle [9]. With these assumptions in mind, a key observation from

Table 3.2. Simulation Materials

Simulation Run Correlation	
Run	Material
1	Brain Tissue
2	Sample 4
3	Sample 3
4	Sample 2
5	Sample 1
6	Aluminum

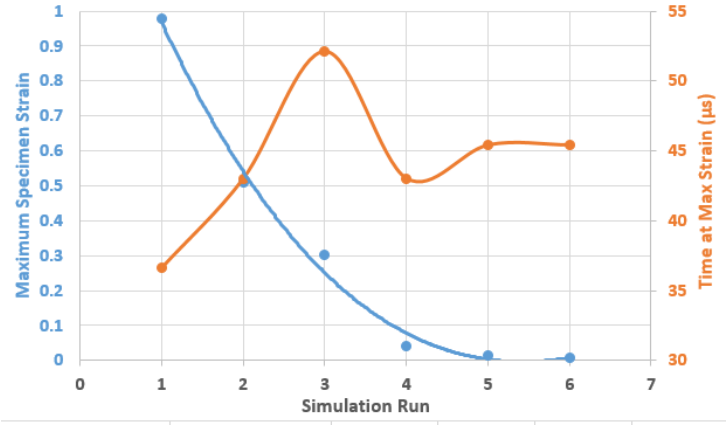

Figure 3.10. Monitoring Maximum Strain Analysis

Figure 3.10 is that unless failure occurs before completion, the maximum buildup of stress commonly occurs between 43 and 46 μs. Even when failure occurs, the maximum stress buildup is not at the instant the simulation fails; however, it is a few timesteps earlier. This observation is important, because it highlights the function of the transmission bar. The free movement of the transmission bar allows this buildup to maximize and then dissipates this energy by continuing to move even when incident bar has stopped moving.

3.7 Testing Yielding in Pulse Shaper

The primary way to understand and confirm the yielding in the pulse shaper is to derive a stress-strain plot for the elements at the core of the pulse shaper in the few time steps before it yields and compare it to the published results of copper material properties. This can be the only way to verify that the pulse shaper is functioning as needed. The location of the pulse shaper can be adjusted from between the striker and the incident bar to either side of the specimen to find an optimal location for the pulse shaper.

Chapter 4

Computational Modeling Results

After the model was confirmed, the specimen was changed from aluminum to experimental values for a brain tissue specimen. This case was compared and contrasted to a similar collision test done on the engineering material to assess any deviation from a uniaxial stress state.

4.1 Aluminum Testing

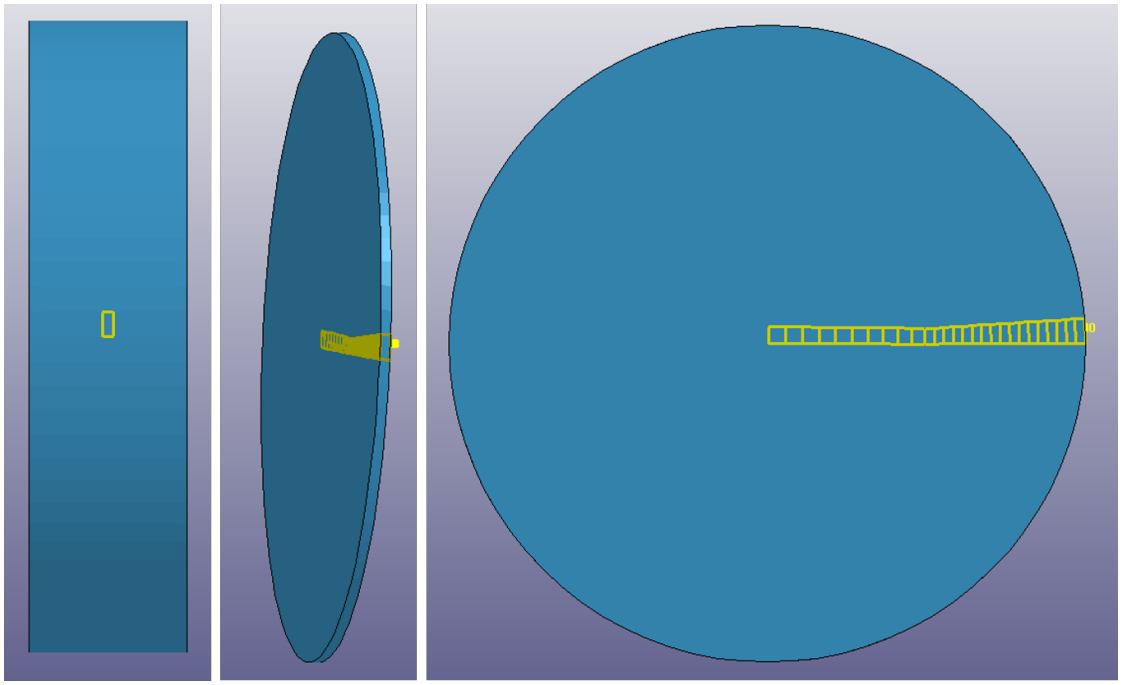

Figure 4.1. Establishing Baseline Uniaxial Stress State for Specimen

Once that preliminary tests showed that the model was physically viable, the next step was to test stresses. In order to do a meaningful analysis all the stress state of the specimen, certain points were carefully picked to avoid inconsistencies, distortion effects, and random sampling noise. As a result, twenty seven elements along the central wedge of the specimen were selected for further analysis.

For these 27 elements the stress was measured at all times in a binary file output by LS-DYNA. Using the code outlined in Appendix B, the raw data was converted to the graphs you see below. The graph in the left half of Figure 4.1 shows that complete stress state for an aluminum specimen at the time that the stresses reach a maxima. From this graph, one can deduce that a majority of the stress is contained in the blue line signifying the axial direction. Stresses in the other primary directions and shears are all close to zero. Another interesting thing to note is that the axial stress becomes less compressive and is in the 400-500 MPa range. This range and trend is important when comparing soft materials to traditional engineering materials.

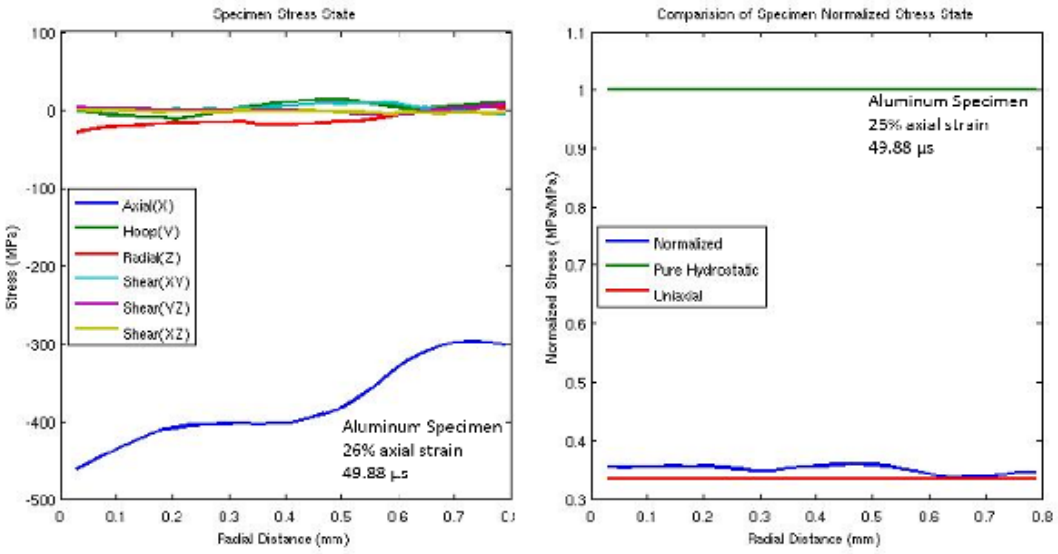

Figure 4.2. Establishing Baseline Uniaxial Stress State for Aluminum

From this complete stress state, a normalized stress is computed using the following equation:

$$\sigma_{norm} = \frac{\sigma_{axial} + \sigma_{hoop} + \sigma_{radial}}{3 * \sigma_{axial}} \tag{4.1}$$

The graph in the right half of Figure 4.2 shows this normalized stress for the

aluminum specimen. The blue line shows the specimen data, but there are two other lines for comparison. If hoop and radial stress was zero, this would represent the ideal case and the red line in the graph at 1/3. If all primary stresses were equal, this would represent the worst possible case and the green line in the graph at 1. Given that the model's normalized stress state is close to the ideal case, we can verify the model's predictive capabilities and proceed to analyzing soft materials.

4.2 Qualitative and Quantitative Analysis of Soft Material Compression Testing

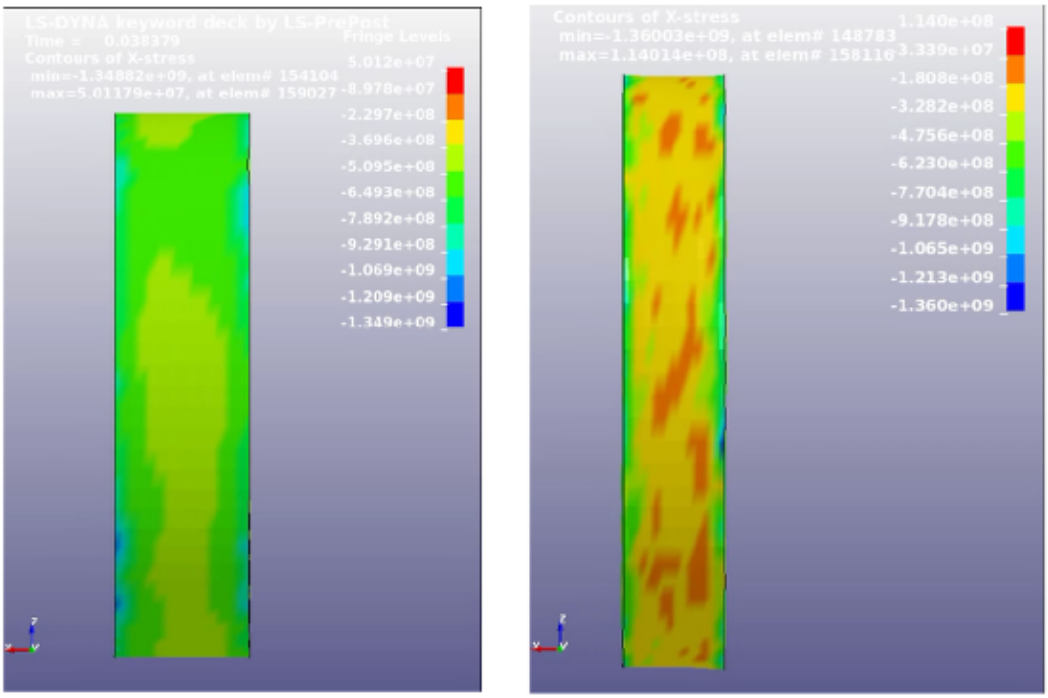

Figure 4.3. Visual Inspection of Soft Material Deformation

Given the viability of the model and some baseline aluminum testing, the material properties of the specimen were changed from aluminum to brain tissue. The first indication of deviation from a simply uniaxial stress can be seen above in Figure 4.3. It shows the end state of an aluminum specimen on the left and soft material on the right. They were pictured to start at the same vertical length and

horizontal thickness. At the end of the compression test, one can visibly see not only more compression in the horizontal (axial) direction as well as excess deformation in the vertical (hoop) direction. Similar inertial effects can also be seen in the radial direction. In addition to visual test, another more quantitative method was also used to compare aluminum to soft materials.

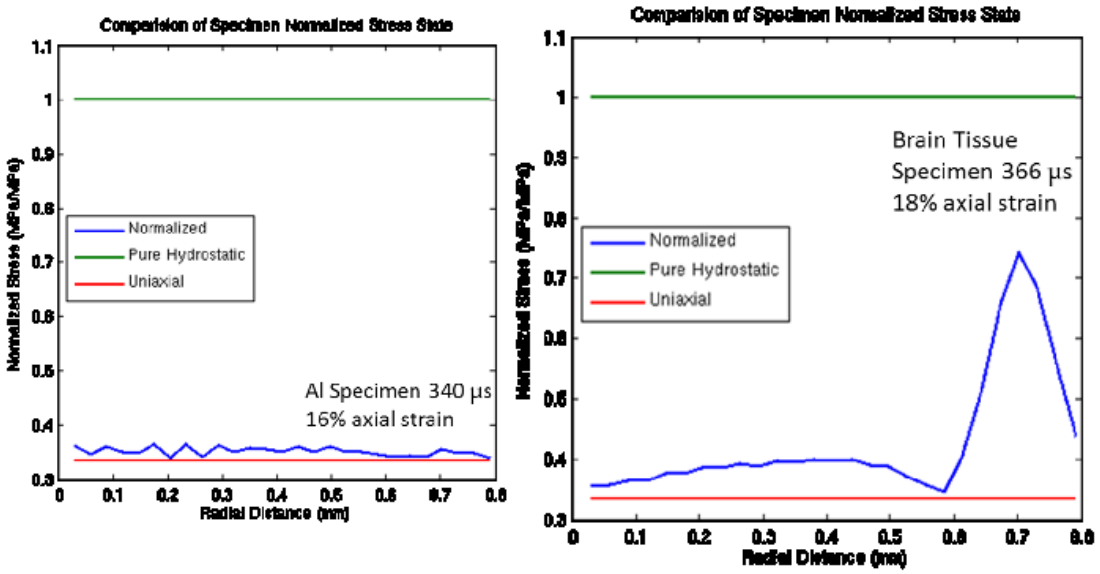

Figure 4.4. Deviation from Uniaxial Stress State in Soft Material Testing

The normalized stress analysis described in Equation 2 was used to get a similar plot of a measure of the uniaxial nature of the stress state in a soft material. In Figure 4.4, this normalized stress state for the soft material is shown on the right and for aluminum is on the left. Comparing these two graphs, the uniaxial stress state assumption holds somewhat for the inner two-thirds of the specimen, but is inaccurate for the outer third. Other tests done by the Army Research Lab on full sized Kolsky bars have achieved a stress state around the 0.7-0.8 range for most of the specimen [7]. Therefore, the miniaturization is a step in the right direction which pulls the specimen's normalized stress state closer to the red line, but more research is necessary to optimize this process. The outer third of the specimen will be our prime area of focus moving on.

4.3 Aluminum to Brain Tissue Transition

Understanding the behavior of materials between standard engineering and soft biological models is pivotal to establishing a constitutive model for the Kolsky bar miniaturization. One of the challenges of this model are to validate all of the computational results and one of the basic ways to do that is to validate the model close to the analysis of engineering materials and extrapolate from there.

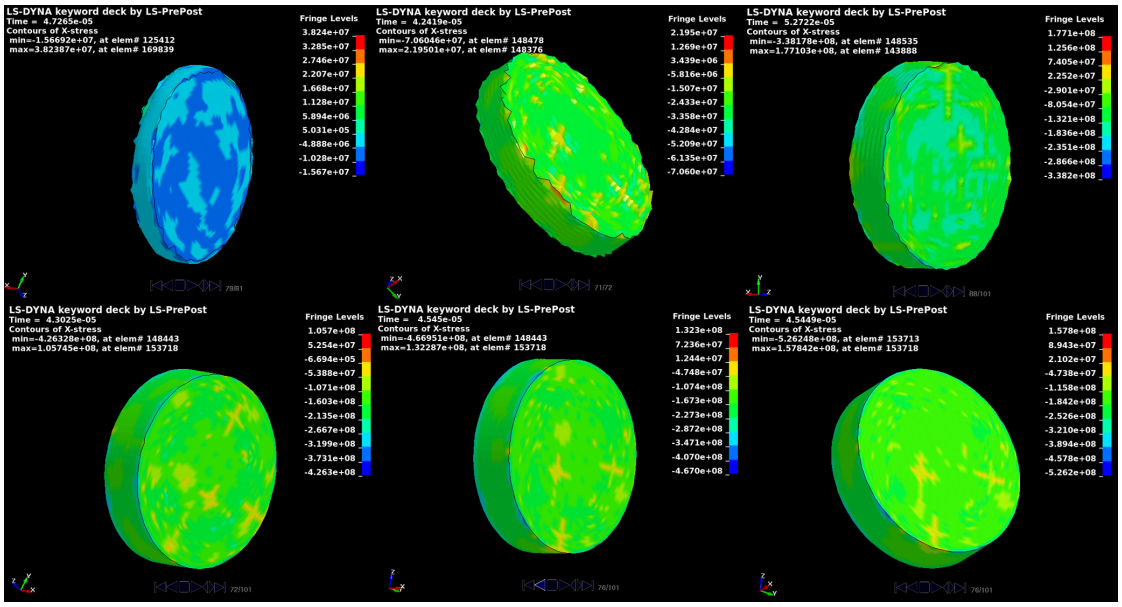

Figure 4.5. Snapshots of Maximum Compression for Six Sample Materials

A general view of the qualitative analysis of the differences between the different simulations will provide a background for the numerical analysis to follow. Pictured in Figure 4.5 are the most compressed snapshot of each of the six simulations starting with brain tissue on the top left and ending with aluminum on the bottom right. In addition to the decreasing compressibility as you move from brain tissue to aluminum, the ranges for the axial stress pictured in the top right corner are also important. With each frame starting with the brain tissue in the top left the stress loaded onto the specimen increases ranging the maximum stress from 15 MPa to 526 MPa. This maximum change can be directly attributed to the changing Young's modulus but is also a function of Poisson's ratio.

Moving on from the quantitative analysis within the finite element model, a deeper understanding of what occurs during the transition from soft material to engineering materials with all of the applicable numbers allows us to analyze which

part of the specimen is really facing the largest deviation from uniaxial loading. As seen from previous work in the preliminary analysis the inner two-thirds of the specimen were really the problematic areas within the Kolsky bar with larger bars. The miniaturized model as pictured here passes that criterion in the uniaxiality test staying close to a 0.4 normalized stress which is close enough to the ideal of 0.33. However, the outer third of the model which has been shown to be accurate in previous work experiences a spike in the loading. When seen across the materials picked for these simulations as shown in Figure 4.6, the specimen for brain tissue as well as sample 4 and sample 3 show a significant deviation from the stress state. Analyzing this difference also explains that this spike in the outer third of the specimen seems to dissipate as you move closer to engineering materials. Whether it is caused by the Young's modulus or Poisson's ratio, the critical takeaway here is the diminishing of this spike as the specimen material becomes nearly incompressible.

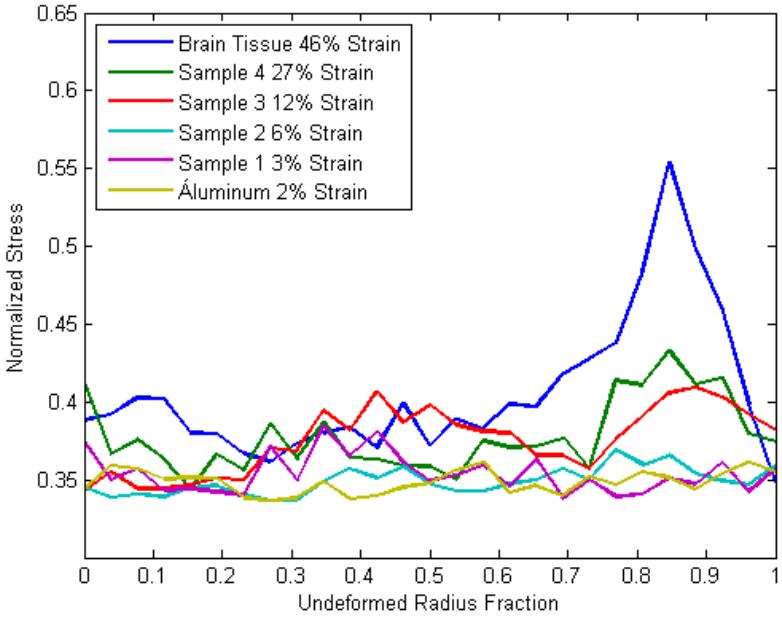

Figure 4.6. Uniaxiality along the Transition from Brain Tissue to Aluminum

Another interesting note is to observe the decreasing strain at which the sample had to be taken. The difference between the moduli of the bar and the sample is one of the key reasons strain builds up in the specimen and this diminishes as the moduli merge to be equal for the case of aluminum. The interesting benefit from a

feasibility standpoint is that having higher value of the strains gives a little more room for fluctuations and error. In addition to using high fidelity strain gages, having a high strain rather than a low one will produce lower percentage errors. Even with sample 4, the buildup of strain is pretty apparent qualitatively and quantitatively, so this machine should remain effective with tissue that is stiffer than brain tissue also.

4.4 Refining Model Sectioning Analysis

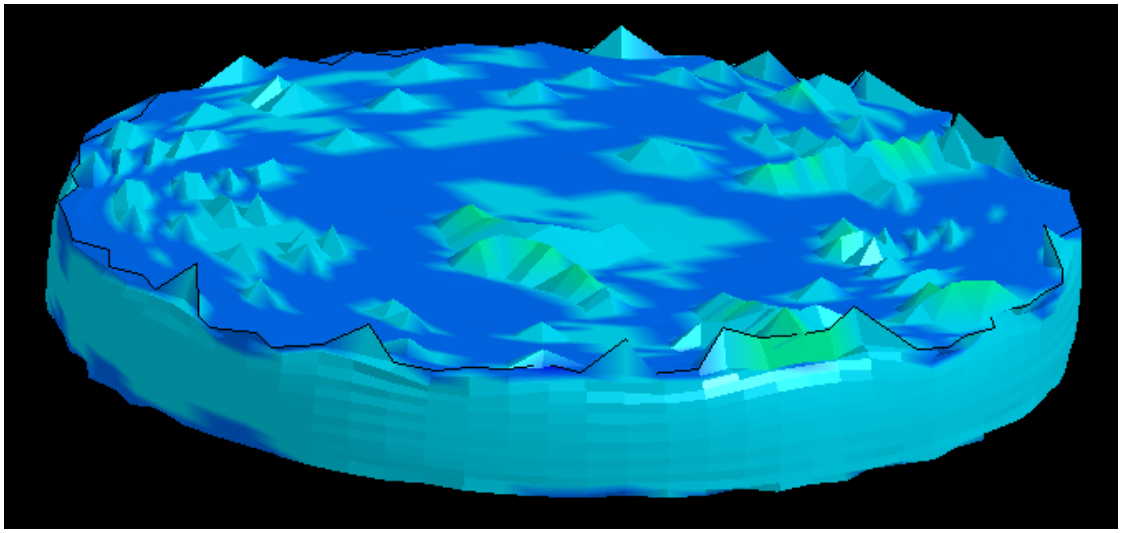

Figure 4.7. Formation of Element Instabilities upon Impact

The transition from engineering materials to soft materials also showed the shortcomings of using LS-DYNA's default constant stress state solid section. For softer materials, this form of analysis does not identify failure or rectify it developing instabilities as pictured in Figure 4.7. Obtaining accurate computational results near the time period of the failure becomes more and more complicated after that.

The LS-DYNA user manual was the most helpful resource in remedying this problem [18]. There are several controls in LS-DYNA that slightly alter the simulation to allow for more accurate results for softer materials. The first resource I used was using a section type that was iterated more frequently over a constant stress state solid. This allowed for adjustments to the code after each iteration to account for element indtabilities in the brain tissue. In conjunction with this

the hourglass feature in LS-DYNA allows for more time steps while the simulation and can be adjusted for blast modeling. A combination of these two methods gave much more accurate results for the stresses and the strains in the softer material modeling. Corotational modeling and ambient Eulerian-Lagrangian principles were also used to get a better handle on the pace at which deformations accrued in soft materials.

Once the soft material compression model was working satisfactorily similar principles were applied to refine the testing of engineering materials as the specimen. Instead of using a nodal approach as was used for the soft materials an eight-nodal approach integrated over each time step was used for the engineering materials. Hourglass stiffness was not an issue for engineering materials, and this analysis smoothed out the response curves for engineering materials providing better resolution and removing oscillations.

4.5 Constitutive Model

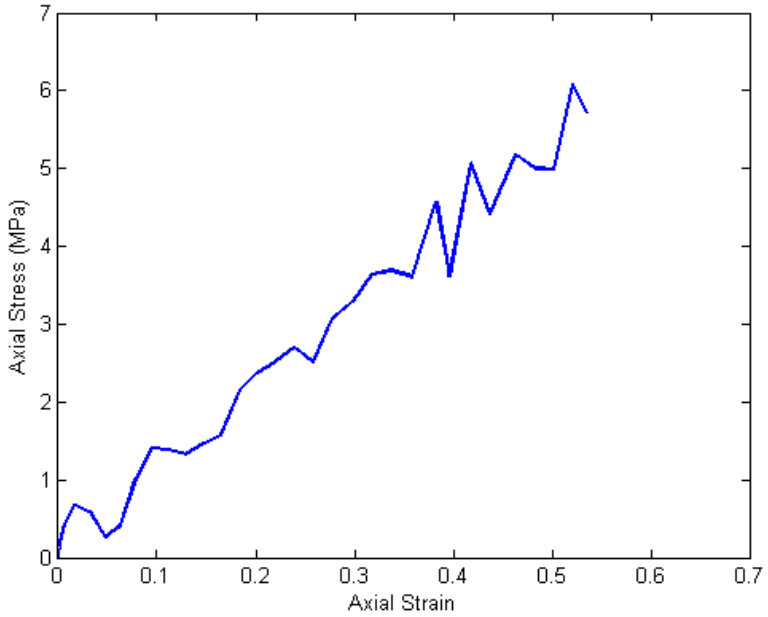

Figure 4.8. Stress Strain Graph of the Brain Tissue Impact

After a more accurate rendering of the model was available, 22 elements on either side of the center of the specimen were examined for their response and

stress strain correlation. The results are plotted in Figure 4.8. Although not a complete constitutive model, this preliminary glance into the stress-strain correlation highlights a few computational strengths of the model. Although there are a few deviations from the prescribed model, a pretty constant slope that matches the input Young's modulus of 10 MPa can be seen in this output. Another important takeaway is the stress at which point failure occurs. The failure of the model occurs at roughly 5.6 MPa, but higher stresses up to 6.02 MPa are reported. This understanding provides more information about the failure mode and can be used to address some of the element instabilities in the LS-DYNA model.

4.6 Analyzing the Feasibility of Pulse Shaping

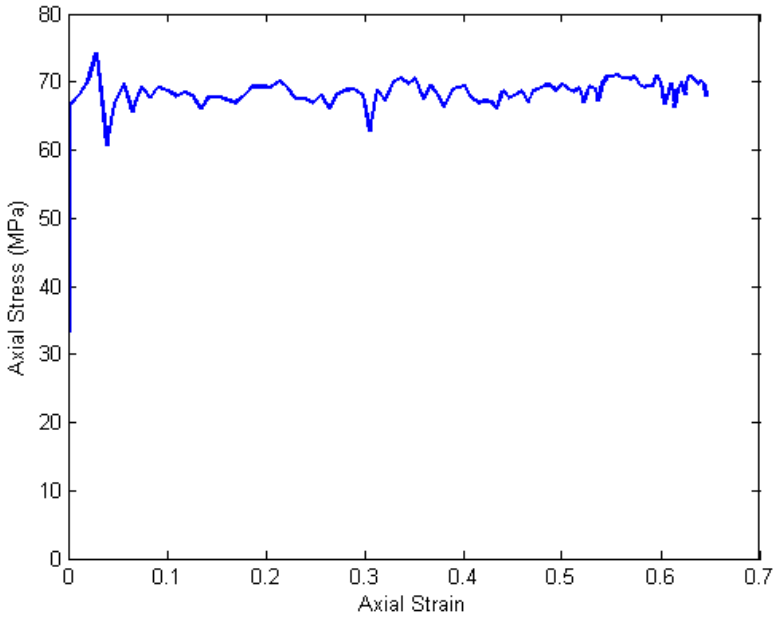

Figure 4.9. Output Stress-Strain Profile of Copper Pulse Shaper

Analyzing our compression results showed that in addition to miniaturizing the model pulse shaping was necessary to optimize the response of brain tissue under high strain rates. In an effort to more closely examine this hypothesis, the yielding of copper placed in between the striker bar and the incident bar was analyzed. Figure 4.9 shows the total response of the copper over the simulation time, and Figure 4.10 shows the elastic region of that response. One of the important things

to note here is that the elastic region in very short lived in time; the majority of the simulation occurs while the copper is yielding and is delaying the immediate transmission of the stress onto the specimen. This yield stress hovers around 68 MPa making copper an ideal choice to pulse shape this specimen of brain tissue. Another possible alternative is changing the criterion of the copper specimen after yielding. Currently, the stress of the copper pulse shaper remains constant while the strain builds up. In order to speed up or delay the transmission of the stress this yield criterion can be changed such that the copper pulse shaper stress decreases or increases as the strain is built up.

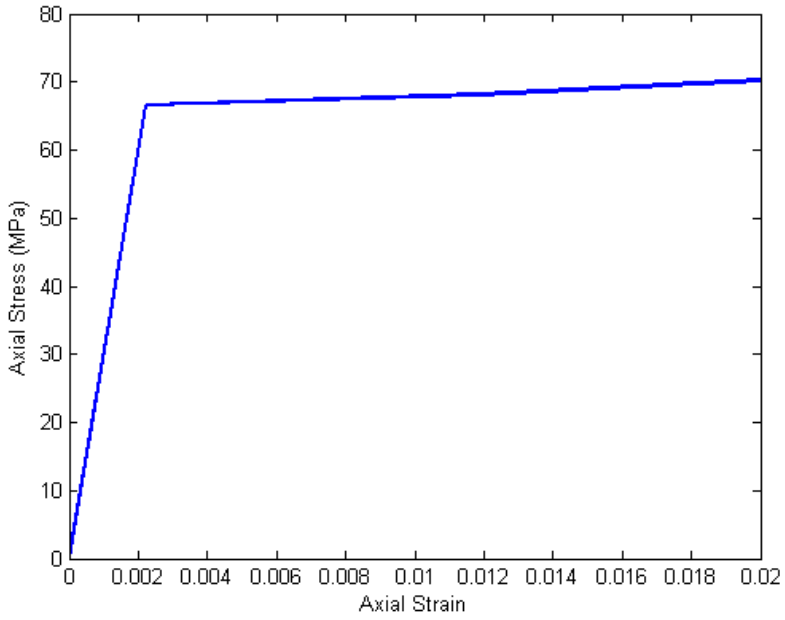

Figure 4.10. Elastic-Plastic Transition for Copper [8]

Continuing onto the simple elastic nature of the copper pulse shaper is another indicator of the desired output. The plastic transition that occurs around 66 MPa and a strain of 0.000055, yields the input material properties of 120 GPa for the copper pulse shaper. Picking a high elastic modulus and yield point allows the copper to absorb the higher ranges of stresses and only allow the correct range of stresses to impact the specimen. Together these modifications and design changes can positively impact the accuracy of today's methods of obtaining soft material propertiesat high strain rates.

Chapter 5

Conclusion

5.1 Discussion

There were a few important takeaways from the process of evaluating the feasibility of the miniaturized model. The first takeaway was the iterative process established to analyze the specimen's stress state. This process can be used to alter attributes of the model to optimize its stress state. Future progress will be more efficient due to the cyclic nature of this process.

The second promising takeaway is positive preliminary results from the miniaturization of the Kolsky bar model. The first comparison of the normalized stress state shows that miniaturization can bring soft material Kolsky bar testing closer to a uniaxial stress state. This supports the belief that inertial effects were causing the deviation from a completely uniaxial stress state. However, more testing is required to verify this for all soft materials and not just brain tissue.

Furthermore, these results allow us to consider other changes to the Kolsky bar apparatus that might be able to bring the stress state closer to uniaxial. Ideas that currently could achieve this include changing the loading type and specimen geometry. The Army Research Lab study got better results with an annular specimen in long bar testing, so it could be one possibility to amend the current model [7]. Another possibility is to change the loading from compression to a double lap shear model, so that a shear component can be the only stress instead of a primary stress component.

Analyzing the transition from soft materials to engineering materials also allowed to identify the high deviation from the uniaxial assumption in the outer

third of the specimen. In addition to prompting a push towards pulse shaping, this allowed us to draw a better understanding of the constitutive model of the brain tissue specimen and its failure. The pulse shaping is feasible at a basic level with the material identified - copper - but a deeper analysis of its impact on the miniaturized model can yield more positive results.

With a deeper understanding of the mechanics of the Kolsky bar compression setup in soft materials, the predictive models used to simulate high strain rate impact on carious parts of the body can be improved. As a result of these improved predictive models, we can help the current treatment of and recuperation from several injuries in civilian environments, professional sports, and even combat zones.

5.2 Future Work

There are two avenues that future work in this endeavor to find more accurate material properties in a cheap and efficient manner could follow.

Using this feasibility study, the first option is to combine pulse shaping and miniaturization to build and test such a device for the compression material properties of brain tissue at high strain rates. This would in turn provide real time data to other students modeling body mechanics and improve their models.

Another opportunity is to capitalize on the double-lap shear mechanism explained in the introductory literature review. While compression material properties to compare computational results to are minimal, shear material properties are almost nonexistent. Catering to this gap in published results a similar undertaking of the feasibility of identifying shear modulus can be another alternative moving forward.

5.3 Application

Even though there is much more possible future work that can be done to accomplish even more refined results for how the brain reacts in high strain rate impact situations, the work undertaken here has potential to make meaningful advances in the understanding and treatment of traumatic brain injuries.

Understanding the typical response of the tissues in and around the head as

well as all over the body in high strain rate situations is an important first step to improving care and rehabilitation for survivors of car crashes, explosions or any other from of concussive impact. Once such a device is manufactured to obtain more accurate material properties for different compressive impacts in soft materials, the opportunities for testing are endless. With data obtained and calibrated computational models from this testing, real-time predictions can be made about the biomechanical applications of various parts of your body. The simple understanding of the basic material properties at high strain rates for soft materials is an important first step in transforming the way treatment and recuperation currently functions for many high strain rate injuries.

Appendix A

Mesh Quality Metrics

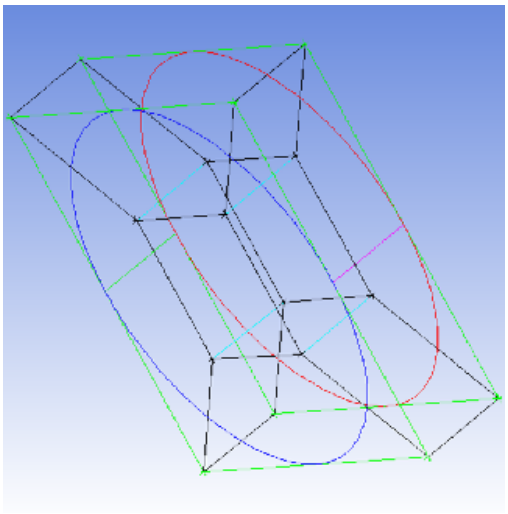

Figure A.1. O-Grid Blocking Pattern for Unstructured Mesh

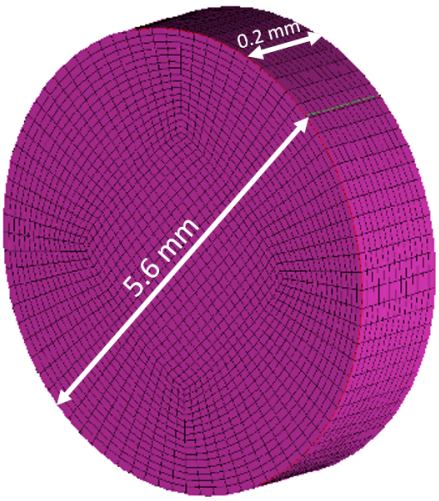

Figure A.2. Complete Volume Mesh of Cylindrical Specimen

Figure A.1 and Figure A.2 show a summary of the blocking mechanisms used for the specimen. In order to understand the metrics used to analyze the mesh shown on the next page, a more thorough understanding of the meshing procedure and its links to the tests can be helpful. The meshing was done using a blocking technique with each dimension along the block acquiring a certain number of nodes. Given the circular nature of the bars and the specimen, an increase in the number of nodes would correlate directly with orthogonality between the elements and the angles necessary to make the elements fit together. However, having a greater number of nodes would also mean longer computation time, and this was not feasible for

more complicated section analysis. With these constraints in mind the meshes for all of the parts combined into an assemble are charted below.

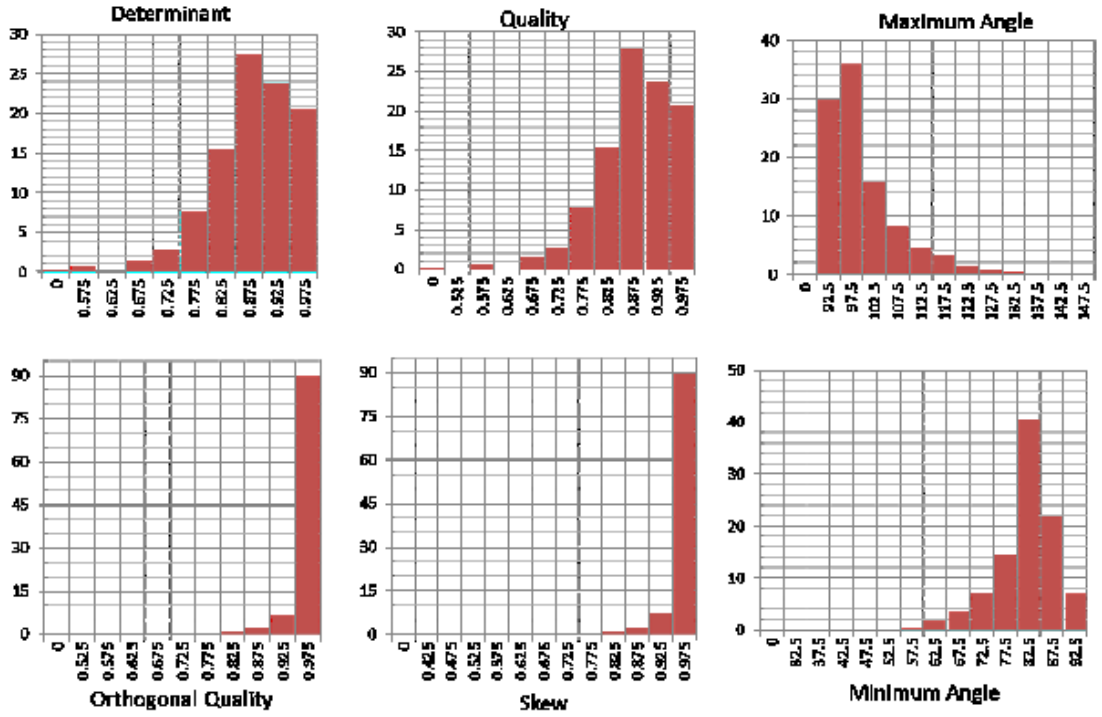

Figure A.3. Six Important Mesh Quality Metrics for Bars and Specimen

Figure A.3 shows the six different metrics shown and histograms of these metrics along the entire Kolsky bar model. For most of these metrics a normal distribution skewed to the higher end of the spectrum with a peak at 80% of the measured values was considered an ideal compromise between accuracy and simulation time. In the case of minimum angle, a peak at 20% of the measured values was desirable. Before beginnin any dynamic simulation this test was rerun to confirm these predicted values.

Appendix B

Finite Element Analysis and MATLAB Code

B.1 LS-DYNA Keyword File

This LS-DYNA k file code demonstrates all of the required values for individual settings in LS-Dyna. Setting and altering these was a major portion of understanding how different theoretical aspects of physics impacted the modeling efforts and are hereby included for reproducibility.

```
|| LS-DYNA Keyword file created by LS-PrePost(R) V4.3 (Beta) - 08Jun2015(19:00)
|| Created on Mar-30-2016 (20:28:50)
*KEYWORD
*TITLE
||                                                                        title
LS-DYNA keyword deck by LS-PrePost
*CONTROL_ENERGY
|     HEGN      RWEN    SLNTEN     RYLEN
||    hgen      rwen    slnten     rylen
         2         2         2         1
*CONTROL_HOURGLASS
|      IHQ        QH
||     ihq        qh
         1       0.1
```

```
*CONTROL_MPP_DECOMPOSITION_DISTRIBUTE_ALE_ELEMENTS
*CONTROL_OUTPUT
|    NPOPT    NEECHO    NREFUP    IACCOP     OPIFS    IPNINT    IKEDIT    IFLUSH
||   npopt    neecho    nrefup    iaccop     opifs    ipnint    ikedit    iflush
         1         3         0         0       0.0         0         0         0
||   iprtf    ierode     tet10    msgmax    ipcurv      gmdt   ip1dblt      eocs
         0         0         2         0         0       0.0         0         0
||   tolev    newleg    frfreq     minfo    solsig    msgflg    cdetol
         2         0         1         0         0         0      10.0
*CONTROL_SHELL
|   WRPANG     ESORT     IRNXX    ISTUPD    THEORY       BWC     MITER      PROJ
||  wrpang     esort     irnxx    istupd    theory       bwc     miter      proj
       0.0         1         0         0         2         2         1         0
|| rotascl    intgrd    lamsht    cstyp6    tshell
       0.0         0         0         0         0
|| psstupd   sidt4tu     cntco    itsflg    irquad
         0         0         0         0         2
||  nfail1    nfail4   psnfail    keepcs     delfr   drcpsid    drcprm
         0         0         0         0         0         0       1.0
*CONTROL_TERMINATION
|   ENDTIM    ENDCYC     DTMIN    ENDENG    ENDMAS
||  endtim    endcyc     dtmin    endeng    endmas
6.00000E-5         0       0.0       0.0       0.0
*CONTROL_TIMESTEP
|   ENDTIM    ENDCYC     DTMIN    ENDENG    ENDMAS
||  dtinit    tssfac      isdo    tslimt     dt2ms      lctm     erode     ms1st
       0.00.89999998         0       0.0       0.0         0         0         0
||  dt2msf   dt2mslc     imscl    unused    unused     rmscl
       0.0         0         0                         0.0
*DATABASE_ABSTAT
||      dt    binary      lcur     ioopt
     0.001         2         0         1
*DATABASE_ELOUT
||      dt    binary      lcur     ioopt   option1   option2   option3   option4
```

```
6.00000E-7         0         0         1         0         0         0         0
*DATABASE_GLSTAT
||      dt    binary      lcur     ioopt
     0.001         0         0         1
*DATABASE_MATSUM
||      dt    binary      lcur     ioopt
     0.001         0         0         1
*DATABASE_RWFORC
||      dt    binary      lcur     ioopt
     0.001         0         0         1
*DATABASE_BINARY_D3PLOT
|   ENDTIM    ENDCYC     DTMIN    ENDENG    ENDMAS
||      dt      lcdt      beam     npltc    psetid
       0.0         0         0       100         0
||   ioopt
         0
*DATABASE_BINARY_D3THDT
|       dt      lcdt      beam     npltc    psetid    istats    tstart      iavg
||      dt      lcdt      beam     npltc    psetid
       1.0         0         0         0         0
*DATABASE_BINARY_INTFOR
|       dt      lcdt      beam     npltc    psetid    istats    tstart      iavg
||      dt      lcdt      beam     npltc    psetid
       1.0         0         0         0         0
||   ioopt
         0
*DATABASE_EXTENT_BINARY
||   neiph     neips    maxint    strflg    sigflg    epsflg    rltflg    engflg
         0         0         3         1         1         1         1         1
||  cmpflg    ieverp    beamip     dcomp      shge     stssz    n3thdt   ialemat
         0         0         0         1         1         1         2         1
|| nintsld   pkp_sen      sclp     hydro     msscl     therm    intout    nodout
         0         0       1.0         0         0         0STRESS    STRESS
||    dtdt    resplt
```

```
         0         0
*DATABASE_HISTORY_SOLID_SET
||     id1       id2       id3       id4       id5       id6       id7       id8
         1         0         0         0         0         0         0         0
*BOUNDARY_SPC_SET
||    nsid       cid      dofx      dofy      dofz     dofrx     dofry     dofrz
         5         0         0         1         1         1         1         1

*CONTACT_AUTOMATIC_GENERAL
||     cid                                                                title
||    ssid      msid     sstyp     mstyp    sboxid    mboxid       spr       mpr
         0         0         0         0         0         0         1         0
||      fs        fd        dc        vc       vdc    penchk        bt        dt
       0.0       0.0       0.0       0.0       0.0         0       0.01.00000E20
||     sfs       sfm       sst       mst      sfst      sfmt       fsf       vsf
       1.0       1.0       0.0       0.0       1.0       1.0       1.0       1.0
*PART
|name
||                                                                         title
TRANSMISSION_BAR
||     pid     secid       mid     eosid      hgid      grav    adpopt      tmid
         1         1         1         0         0         0         0         0
*SECTION_SOLID
|       id   elformu       aet
||   secid    elform       aet
         1         1         4
*MAT_ELASTIC
|      MID        RO         E        PR        DA        DB         K
||     mid        ro         e        pr        da        db  not used
         1    2712.06.90000E100.33399999       0.0       0.0         0
*PART
|name
||                                                                         title
SPECIMEN
```

```
||     pid     secid       mid     eosid      hgid      grav    adpopt      tmid
         2         2         2         0         0         0         0         0
*SECTION_SOLID
||   secid    elform       aet
         2         1         4
*MAT_ELASTIC
|      MID        RO         E        PR        DA        DB         K
||     mid        ro         e        pr        da        db  not used
         2    1000.0 10370000.0.49000001       0.0       0.0         0
*PART
|name
||                                                                   title
INCIDENT_BAR
||     pid     secid       mid     eosid      hgid      grav    adpopt      tmid
         3         3         1         0         0         0         0         0
*SECTION_SOLID
||   secid    elform       aet
         3         1         4
*PART
|name
||                                                                   title
STRIKER_BAR
||     pid     secid       mid     eosid      hgid      grav    adpopt      tmid
         4         4         1         0         0         0         0         0
*SECTION_SOLID
||   secid    elform       aet
         4         1         4
*INITIAL_VELOCITY_GENERATION
||nsid/pid      styp     omega        vx        vy        vz     ivatn      icid
         4         2       0.0-5.5999999       0.0       0.0         0         0
||      xc        yc        zc        nx        ny        nz     phase    irigid
       0.0       0.0       0.0       0.0       0.0       0.0         0         0
*DEFINE_CURVE
||    lcid      sidr       sfa       sfo      offa      offo    dattyp     lcint
```

```
         1         0       1.0       1.0       0.0       0.0         0         0
||               a1                  o1
                0.0                 0.0
                0.2                 0.0
*DEFINE_CURVE
||    lcid      sidr       sfa       sfo      offa      offo    dattyp     lcint
         2         0       1.0       1.0       0.0       0.0         0         0
||               a1                  o1
                0.0                 1.0
                0.2                 1.0
*DEFINE_CURVE
||    lcid      sidr       sfa       sfo      offa      offo    dattyp     lcint
         3         0       1.0       1.0       0.0       0.0         0         0
||               a1                  o1
                0.0                 0.0
                0.2                 1.0
                1.0                 1.0
*DEFINE_CURVE
||    lcid      sidr       sfa       sfo      offa      offo    dattyp     lcint
         4         0       1.0       1.0       0.0       0.0         0         0
||               a1                  o1
                0.0                 0.0
                0.2                 0.0
*SET_NODE_LIST_TITLE
```

B.2 MATLAB Code

In addition to the LS-DYNA code another important benchmark used to analyze all of the data received from simulations through LS-DYNA was MATLAB. This MATLAB code is used to find and plot the normalized stress as well as the several different components of stress as shown in Figure 4.2.

```
M = csvread('Incident_Bar_Axial_Stress.csv', 1,0);
N = csvread('Transmitted_Bar_Axial_Stress.csv', 1,0);
```

```
O = csvread('Transmitted_Bar_Velocity.csv', 1,0);
P = csvread('Incident_Bar_Velocity.csv', 1,0);
d_i = M(:,1);
S_i = M(:,2);
d_t = N(:,1);
S_t = N(:,2);
t = O(:,1);
time = 1e3*t;
vel_t = O(:,2:7);
vel_i = P(:,2:7);
for a = 1:1:17;
    dist_i(a) = mean(d_i((3*a-2):3*a));
    Stress_i(a) = mean(S_i((3*a-2):3*a));
    dist_t(a) = mean(d_t((3*a-2):3*a));
    Stress_t(a) = mean(S_t((3*a-2):3*a));
end
for b = 1:1:101
    velocity_t(b) = mean(vel_t(b,1:6));
    velocity_i(b) = mean(vel_i(b,1:6));
end
dist_i = 1000*(dist_i - d_i(27));
Stress_i = 1e-6*Stress_i;
dist_t = 1000*(dist_t - d_t(27));
Stress_t = 1e-6*Stress_t;
figure
plot(dist_i,Stress_i,'-ro',dist_t,Stress_t,'-.b','LineWidth',2);
xlabel('Radius (mm)')
ylabel('Axial Stress (MPa)')
title('Stress Distribution on Impact Face')
legend('Incident Bar', 'Transmitted Bar','Location','southeast')
figure
plot(time,velocity_t,time,velocity_i,'LineWidth',2)
xlabel('Time (ms)')
ylabel('Axial Velocity (m/s)')
```

```
title('Impact Velocity')
legend('Incident Bar', 'Transmitted Bar')
axis([0 0.06 -2.5 11.5])
fnm=input('Please enter the file name: ','s');
testime=input('What time should the stresses be plotted? ');
numel=input('How many elements are present? ');
mat=csvread(fnm,1,0);
[ro co]=size(mat);
time=mat(:,1);
for n=1:ro
    test=time(n);
    if testime >= test
        elrow = n;
    end
end
xcoord=1:1:numel;
xcoord=xcoord./numel;
xcoord=xcoord.*.79;
effstr=mat(elrow,2:1+numel)./1e6;
sigxx=mat(elrow,2+numel:2*numel+1)./1e6;
tauxy=mat(elrow,2+2*numel:3*numel+1)./1e6;
sigyy=mat(elrow,2+3*numel:4*numel+1)./1e6;
tauyz=mat(elrow,2+4*numel:5*numel+1)./1e6;
tauzx=mat(elrow,2+5*numel:6*numel+1)./1e6;
sigzz=mat(elrow,2+6*numel:7*numel+1)./1e6;
yield=mat(elrow,2+7*numel:8*numel+1)./1e6;
pressure=mat(elrow,2+8*numel:9*numel+1)./1e6;
vmstress=mat(elrow,2+9*numel:10*numel+1)./1e6;
maxprindev=mat(elrow,2+10*numel:11*numel+1)./1e6;
secprindev=mat(elrow,2+11*numel:12*numel+1)./1e6;
minprindev=mat(elrow,2+12*numel:13*numel+1)./1e6;
maxshear=mat(elrow,2+13*numel:14*numel+1)./1e6;
maxprin=mat(elrow,2+14*numel:15*numel+1)./1e6;
secprin=mat(elrow,2+15*numel:16*numel+1)./1e6;
```

```
minprin=mat(elrow,2+16*numel:17*numel+1)./1e6;
norm=(abs(sigxx)+abs(sigyy)+abs(sigzz))./(3*abs(sigxx));
hyd=ones(1,numel);
uni=hyd./3;
figure
subplot(2,2,1)
plot(xcoord,sigxx,xcoord,sigyy,xcoord,sigzz,xcoord,effstr)
title('Plane Stresses')
legend('Axial(X)','Hoop(Y)','Radial(Z)','Effective','Location','best')
xlabel('Radial Distance (mm)')
ylabel('Stress (MPa)')
subplot(2,2,2)
plot(xcoord,tauxy,xcoord,tauyz,xcoord,tauzx,xcoord,maxshear)
title('Shear Stresses')
legend('TauXY','TauYZ','TauZX','Maximum Shear','Location','best')
xlabel('Radial Distance (mm)')
ylabel('Stress (MPa)')
subplot(2,2,3)
plot(xcoord,maxprindev,xcoord,secprindev,xcoord,minprindev,xcoord,pressure,
xcoord,yield)
title('Deviatoric Stresses')
legend('Max','II','Min','Pressure','Yield','Location','best')
xlabel('Radial Distance (mm)')
ylabel('Stress (MPa)')
subplot(2,2,4)
plot(xcoord,maxprin,xcoord,secprin,xcoord,minprin,xcoord,vmstress)
title('Principal Stresses')
legend('Max','II','Min','Von Mises','Location','best')
xlabel('Radial Distance (mm)')
ylabel('Stress (MPa)')
figure
x=plot(xcoord,sigxx,xcoord,sigyy,xcoord,sigzz,xcoord,tauxy,xcoord,tauyz,
xcoord,tauzx,'LineWidth',2);
title('Specimen Stress State')
```

```
legend('Axial(X)','Hoop(Y)','Radial(Z)','Shear(XY)','Shear(YZ)','Shear(XZ)',
'Location','west')
xlabel('Radial Distance (mm)')
ylabel('Stress (MPa)')
figure
plot(xcoord,norm,xcoord,hyd,xcoord,uni,'LineWidth',2)
title('Comparision of Specimen Normalized Stress State')
legend('Normalized','Pure Hydrostatic','Uniaxial','Location','west')
xlabel('Radial Distance (mm)')
ylabel('Normalized Stress (MPa/MPa)')
axis([0 0.8 0.3 1.1])
```

Bibliography

[1] Chen, W. W. and B. Song (2011) "Split Hopkinson (Kolsky) Bar: Design, Testing and Applications," chap. 1, 2, and 4, Springer, New York.

[2] Ott, K. A., R. Armiger, A. Wickwire, A. Iwaskiw, and A. C. Merkle (2012) "Determination of simple shear material properties of the brain at high strain rates," in *Dynamic Behavior of Materials, Volume 1: Proceedings of the 2012 Annual Conference on Experimental and Applied Mechanics*, Springer Science & Business Media, p. 139.

[3] Song, B. and W. Chen (2005) "Split Hopkinson pressure bar techniques for characterizing soft materials," *Latin American Journal for Solids and Structures*, **2**, pp. 113–152.

[4] The Slow Mo Guys (2010), "Football to the Face in Slow Motion," .

[5] Roan, E. and K. Vemaganti (2007) "The Nonlinear Material Properties of Liver Tissue Determined from No-Slip Uniaxial Compression Experiments," *Journal of Biomechanical Engineering*, **129**(3), pp. 450–456.

[6] Weed, B. C., A. Borazjani, R. Patnaik, S. S .and Prabhu, M. F. Horstemeyer, P. L. Ryan, T. Franz, L. N. Williams, and J. Liao (2012) "Stress State and Strain Rate Dependence of the Human Placenta," *Annals of Biomedical Engineering*, **40**(10), pp. 2255–2265.

[7] Scheidler, M., J. Fitzpatrick, and R. Kraft (2011) "Optimal pulse shapes for SHPB tests on soft materials," in *Dynamic Behavior of Materials, Volume 1*, Springer, pp. 259–268.

[8] Copper Development Association Inc. (2016) "Application Data Sheet: Mechanical Properties of Copper and Copper Alloys," *Copper Alliance*.

[9] Southwest Research Institute (2006) "Split-Hopkinson Pressure Bar Apparatus," *American Society of Mechanical Engineers*, pp. 2–4, from `asme.org/getmedia/a82d72ab-e923-4aa9-ac3fb7463a/242-Split-Hopkinson-Pressure-Bar-Apparatus.aspx`.

[10] Lorenzo, J. "Elastic Moduli and Physical Properties of Rocks," in *Petroleum Seismology*, chap. 6.

[11] Ramesh, K. T. "High Strain Rate and Impact Experiments," in *Springer Handbook for Solid Mechanics*, pp. 3–13.

[12] Field, J. E., H. T. Goldrein, W. G. Proud, C. R. Siviour, and S. M. Walley (2004) "Review of experimental techniques for high rate deformation and shock studies," *International Journal of Impact Engineering*, **30**, pp. 729–734.

[13] Trexler, M., A. Lennon, A. Wickwire, T. Harrigan, Q. Luong, J. Graham, A. Maisano, J. Roberts, and A. Merkle (2011) "Verification and implementation of a modified split Hopkinson pressure bar technique for characterizing biological tissue and soft biosimulant materials under dynamic shear loading," *Journal of the mechanical behavior of biomedical materials*, **4**(8), pp. 1920–1928.

[14] Destrade, M., M. Gilchrist, and B. Rashid "A High Rate Tension Device for Characterizing Brain Tissue," **1302**(4175), pp. 1–3, from `arxiv.org/ftp/arxiv/papers/1302/.pdf`.

[15] Coronado, V., M. Faul, M. M. Wald, and L. Xu (2010) *Traumatic Brain Injury in the United States*, Centers for Disease Control and Prevention, from `cdc.gov/traumaticbraininjury/pdf/blue_book.pdf`.

[16] Mollica, F., L. Preziosi, and K. R. Rajagopal (2006) "Modeling of biological materials," *Birkhauser, Boston, Massachusetts, Chap.*, **1**.

[17] Casem, D., V. Chalivendra, and B. Song (2013) "Dynamic Behavior of Materials," in *Volume 1: Proceedings of the 2012 Annual Conference on Experimental and Applied Mechanics*, chap. 5, Springer, New York.

[18] LSTC, Inc and DYNAmore GmbH (2015) "Elements," in *LS-DYNA User's Guide*, LS-DYNA Support, from `http://www.dynasupport.com/tutorial/ls-dyna-users-guide/elements`.

[19] Barber, T. W., J. A. Brockway, and L. S. Higgins (1970) "The Density of Tissues in and about the Head," *Acta Neurologica Scandinavica*, **46**, pp. 85–92.

[20] Schiavone, P., F. Chassat, T. Boudou, E. Promayon, F. Valdivia, and Y. Payan (2009) "In vivo measurement of human brain elasticity using a light aspiration device," *Medical image analysis*, **13**(4), pp. 673–678.

[21] Lippert, S. A. and M. J. Grimm (2003) "Estimating the material properties of brain tissue at impact frequencies: A curve-fitting solution," in *Summer Bioengineering Conference, Key Biscayne, Florida*, from `http://www.tulane.edu/~sbc2003/pdfdocs/0125.PDF`.

Academic Vita of Kush Sodha

kbs5154@psu.edu | (732) 910-9552 3420 Stafford Pl | Southampton, PA 18966

Education

Bachelor of Science in Mechanical Engineering May 2016
The Pennsylvania State University
Minoring in Engineering Entrepreneurship & Engineering Mechanics
Schreyer Honors College, College of Engineering Dean's List

Research Experience

Penn State College of Engineering Research Experience for Undergraduates *July 2015*

- Published article and short presentation on high strain rate soft material properties

American Society of Mechanical Engineers IMECE Design Expo Poster *November 2015*

- Presented poster on novel design to adapt Kolsky bar to soft materials at high strain rates

Engineering Experience

Research Assistant, Penn State Computational Biomechanics Group *Fall 2014-Present*

- Led a feasibility study of miniaturized Split Hopkinson Pressure Bar to more accurately estimate material properties of soft materials like brain tissue under high strain rates
- Preliminary results show miniaturized bars made of a softer metal, aluminum, can obtain comparable high strain rate properties for soft materials in a cost effective manner

Transmission Modeling and Simulation Lead, Penn State EcoCAR 3 *Fall 2015-Present*

- Managed efforts to test the Transmission Control Module and its algorithm for performance and emissions while assigning deadlines and budgeting through Microsoft Project
- Generated code for engine and transmission software electronic control units (SoftECUs)
- Coordinated modeling efforts with transmission packaging and wiring harnesses

Technical Skills

Finite Element Analysis

- Advanced practical knowledge of Ansys ICEM-CFD, LS-DYNA, Python, Red Hat Linux, and Solidworks through research efforts in soft material dynamic contact simulation

Simulation and Modeling

- Advanced practical knowledge of Simulink and MATLAB through modeling Software Electronic Control Units. Working knowledge about dSpace ControlDesk and Autonomie

Professional and Volunteer Experience

Teaching Assistant, Center for Engineering Design and Entrepreneurship *Spring 2014-Present*

- Created and led group activities in innovation and new entrepreneurial projects
- Independently evaluated thirty upperclassmen in finance and marketing

Logistics Team Leader, Schreyer Honors College Freshman Orientation *Summer 2014, 2015*

- Coordinated a hundred volunteers and three hundred freshman for three days filled with orientation activities. Mentored a group of ten freshman in orientation activities

Alternative Fundraising Chair, THON Rules and Regulation Committee *Fall 2013-Spring 2015*

- Managed fundraising opportunities for a group of fifty volunteers in the fight against pediatric cancer. Created innovative events and revamped existing programs

Teaching Assistant, Philadelphia Futures *Summer 2013*

- Educated a group of inner city youth tasked to make business plans with Dr. Jonathan Scott at Temple University. Added new, challenging exercises to their curriculum

Awards

Council Rock High School North Distinguished Scholar | Bucks County Courier Times Dick Dougherty Scholarship | William Schreyer Scholarship | Barbara and Philip Schumacher Scholarship | Microsoft Office Specialist (Word, Excel, Access, PowerPoint)